SERI/TR-252-2718
UC Category: 59a
DE86004448

SERI Desiccant Cooling Test Facility: Status Report

Preliminary Data on the Performance of a Rotary Parallel-Passage Silica-Gel Dehumidifier

Kenneth J. Schultz

April 1986

Prepared under Task No. 3023.21
FTP No. 01-548-85

Solar Energy Research Institute
A Division of Midwest Research Institute

1617 Cole Boulevard
Golden, Colorado 80401-3393

Prepared for the
U.S. Department of Energy
Contract No. DE-AC02-83CH10093

Printed in the United States of America
Available from:
National Technical Information Service
U.S. Department of Commerce
5285 Port Royal Road
Springfield, VA 22161

Price: Microfiche A01
Printed Copy A04

Codes are used for pricing all publications. The code is determined by the number of pages in the publication. Information pertaining to the pricing codes can be found in the current issue of the following publications, which are generally available in most libraries: *Energy Research Abstracts, (ERA); Government Reports Announcements* and Index (*GRA* and I); *Scientific and Technical Abstract Reports (STAR);* and publication, NTIS-PR-360 available from NTIS at the above address.

PREFACE

In keeping with the national energy policy goal of fostering an adequate supply of energy at a reasonable cost, the United States Department of Energy (DOE) supports a variety of programs to promote a balanced and mixed energy resource system. The mission of the DOE Solar Buildings Research and Development Program is to support this goal by providing for the development of solar technology alternatives for the buildings sector. It is the goal of the program to establish a proven technology base to allow industry to develop solar products and designs for buildings that are economically competitive and can contribute significantly to the nation's building energy supplies. Toward this end, the program sponsors research activities related to increasing the efficiency, reducing the cost, and improving the long-term durability of passive and active solar systems for building water and space heating, cooling, and daylighting applications. These activities are conducted in four major areas: Advanced Passive Solar Materials Research, Collector Technology Research, Cooling Systems Research, and Systems Analysis and Applications Research.

Advanced Passive Solar Materials Research - This activity area includes work on new aperture materials for controlling solar heat gains, and for enhancing the use of daylight for building interior lighting purposes. It also encompasses work on low-cost thermal storage materials that have high thermal storage capacity and can be integrated with conventional building elements, and work on materials and methods to transport thermal energy efficiently between any building exterior surface and the building interior by nonmechanical means.

Collector Technology Research - This activity area encompasses work on advanced low- to medium-temperature (up to 180°F useful operating temperature) flat-plate collectors for water and space heating applications, and medium- to high-temperature (up to 400°F useful operating temperature) evacuated tube/concentrating collectors for space heating and cooling applications. The focus is on design innovations using new materials and fabrication techniques.

Cooling Systems Research - This activity area involves research on high-performance dehumidifiers and chillers that can operate efficiently with the variable thermal outputs and delivery temperatures associated with solar collectors. It also includes work on advanced passive cooling techniques.

Systems Analysis and Applications Research - This activity area encompasses experimental testing, analysis, and evaluation of solar heating, cooling, and daylighting systems for residential and nonresidential buildings. This involves system integration studies, the development of design and analysis tools, and the establishment of overall cost, performance, and durability targets for various technology or system options.

This report documents the current status of the SERI Desiccant Cooling Test Facility and includes preliminary data on the performance of a spirally wound, parallel-passage, rotary dehumidifier using silica gel as the desiccant.

This work was performed under Task 3023.21, Desiccant Cooling Research, during FY 1985. Testing of other rotary dehumidifiers will continue. The author thanks Terry Penney, among others, at SERI, and John Mitchell of the University of Wisconsin for their help and encouragement during this work.

Kenneth J. Schultz

Kenneth J. Schultz

Approved for

SOLAR ENERGY RESEARCH INSTITUTE

David H. Johnson

David Johnson, Manager
Thermal Sciences Research Branch

L. J. Shannon

L. J. Shannon, Director
Solar Heat Research Division

SUMMARY

Objective

This report describes the SERI Desiccant Cooling Test Facility as it now stands and gives preliminary data on a prototype spirally wound, parallel-passage rotary dehumidifier using silica gel as the desiccant.

Discussion

Much analytical and experimental work has been put into rotary desiccant dehumidifiers and desiccant cooling systems. However, there has been little coordination between these two areas. Desiccant dehumidifier models have been used extensively in systems analysis with little experimental verification.

The SERI Desiccant Cooling Test Facility was constructed to remedy this situation. Data on various rotary dehumidifiers that have been obtained from this facility will be used to verify the accuracy of dehumidifier models, providing a new level of confidence in dehumidifier design and desiccant cooling systems analysis.

Conclusions and Recommendations

The SERI Desiccant Cooling Test Facility is operational. Several minor difficulties, including humidity control and inlet velocities, were discussed and improvements were suggested.

We obtained satisfactory data on a prototype parallel-passage silica-gel rotary dehumidifier. Preliminary analysis of the data indicates an effective Lewis number near unity. However, nonuniformities in the passage spacings have reduced the effective number of transfer units by a factor of 3-4.

Construction and testing of a dehumidifier with a matrix of uniform passage spacings are recommended.

TABLE OF CONTENTS

	Page
Nomenclature	ix
1.0 Introduction	1
1.1 Background	1
1.2 Purpose of Test Facility	1
2.0 Description of Test Facility	5
2.1 Overview	5
2.2 General Layout	5
2.2.1 Flow Loop Design	5
2.2.2 Test Unit Design	5
3.0 Data Acquisition and Control System	12
4.0 Controls	15
4.1 Flow Rates	15
4.2 Temperatures	17
4.3 Humidity	17
4.4 Wheel Speed	18
5.0 Instrumentation	19
5.1 Temperature	19
5.2 Humidity	19
5.3 Pressure	23
5.4 Flow Rate	25
5.5 Wheel Speed	25
6.0 Preliminary Data	26
6.1 Description of Dehumidifier Wheel	26
6.2 Seal Leakage Rates	26
6.3 Overall Facility Operation	28
6.4 Initial Tests	32
6.4.1 Low Speed Tests	32
6.4.2 High Speed Tests	37
7.0 Conclusions	41
7.1 Facility Status and Preliminary Test Results	41
7.2 Future Work	41
8.0 References	42
Selected Distribution List	45

LIST OF FIGURES

Page

1-1 The Ventilation Cycle Desiccant Cooling System...................... 2

1-2 The Recirculation Cycle Desiccant Cooling System.................... 3

2-1 Test Facility Layout.. 6

2-2 Desiccant Cyclic Test Facility Looking South to North............... 7

2-3 Desiccant Cyclic Test Facility Looking North to South............... 8

2-4 System Capabilities... 9

2-5 Rotary Dehumidifier in Test Facility with One Transition Section Removed... 11

3-1 Instrumentation and Data Acquisition Center......................... 13

3-2 Data Acquisition Program Flowchart.................................. 14

4-1 Schematic of Control Functions and Required Ranges.................. 15

4-2 Fan Performance Curve... 16

5-1 Measurement Locations... 20

5-2 Thermocouple Design... 23

5-3 Sampling Points to Obtain Outlet Profile............................ 24

6-1 Coating of the Tape Film with Silica Gel............................ 27

6-2 First Test Dehumidifier from Rotary Heat Exchanger, Australia....... 29

6-3 Seal Designs.. 30

6-4 Dehumidifier Seal Leakage Paths..................................... 31

6-5 Low Rotation Speed Outlet States.................................... 34

6-6 F_2 Effectiveness versus C_{2jp}.................................. 36

6-7 Fit to Very Low Speed Data.. 36

6-8 F_2 Effectiveness versus C_{2ja}.................................. 37

6-9 High Speed Test Results... 40

LIST OF TABLES

		Page
1-1	Projected Performance of Advanced Dehumidifier Systems at ARI Design Conditions	3
2-1	Specifications for Flow Loop Air States	6
3-1	Data Acquisition and Control Unit Channel Allocation	12
5-1	Summary of Required Measurements	21
6-1	Parameters of the First Test Dehumidifier	28
6-2	Typical Seal Leakage Rates	31
6-3	Silica Gel and Matrix Properties	34
6-4	Low Rotation Speed Tests	35
6-5	High Rotation Speed Tests	39

NOMENCLATURE

A	moist air
c_p	specific heat of air (kJ/kg ^oC)
c_{pA}	specific heat of moist air
c_{pDD}	specific heat of dry desiccant
c_{pT}	specific heat of tape
c_{pW}	specific heat of water
C	discharge coefficient (dimensionless)
C_{ij}	reciprocal of the dimensionless wave speed for potential i in period j
C_{max}	maximum value of fluid capacity rate in matrix (J/ks or kg/s)
C_{min}	minimum value of fluid capacity rate in matrix (J/ks or kg/s)
C_r	matrix capacity rate (J/ks or kg/s)
C^*	C_{min}/C_{max}
C_r^*	C_r/C_{min}
COP_{th}	thermal coefficient of performance
COP_e	electric coefficient of performance
d	nozzle diameter (m)
D	duct diameter (m)
DA	dry air
DD	dry desiccant
F_i	potential 1 or potential 2
G_f	gain factor, currently set to 1.0 (dimensionless)
G_t	gain factor, currently set to 1.0
h	specific enthalpy of moist air (J/kg dry air)
h_s	heat of adsorption
h_v	latent heat of vaporization of water

NOMENCLATURE (Continued)

j	period 1 (process) or period 2 (regeneration)
K_f	flow equation coefficient (kg-K/s-unit)
K_t	temperature equation coefficient (kW/unit)
K_w	wheel speed control equation coefficient (rph/unit)
K_F	coefficient for the Fincor controller (rpm/mA)
K_{HP}	coefficient for the HP 3497A (mA/unit)
K_S	flow system constant (m^3/s/rpm)
K_{SCR}	coefficient for the SCR controller (kW/mA)
Le_o	effective Lewis number
$\dot{m}$	mass flow rate (kg/s)
$\dot{m}_S$	set point mass flow rate (kg/s)
$\dot{m}_{DA}$	flow rate of dry air (kg/s)
$\dot{m}_{DAj}$	mass flow rate of dry air in period j (kg/s)
m_{DD}	mass of dry gel (kg)
m_{DDa}	active value of m_{DD}
m_{DDp}	physical value of m_{DD}
m_T	mass of tape
N	wheel rotation speed (rph)
N_s	set point wheel speed (rph)
NTU_o	overall number of transfer units
NTU_{to}	NTU_o for sensible heat transfer
NTU_{wo}	NTU_o for moisture transfer
p	indicates calculation is based on physical measurements
P	ambient pressure (Pa)
P_{sat}	saturation vapor pressure (Pa)

NOMENCLATURE (Continued)

P_t	total absolute pressure (Pa)
P_{tot}	atmospheric pressure (Pa)
P_v	equilibrium vapor pressure (atm)
Q	energy input rate (kW)
R	gas constant for air (289.6 J/kg K)
Re_d	Reynolds number at the nozzle throat
S	integer signal from IBM PC to HP 3497A (unit)
S_o	offset signal (unit)
t	temperature (^oC)
t_{amb}	ambient temperature (^oC)
t_s	set point temperature (^oC)
t_{DP}	dew point temperature (^oC)
T	absolute temperature (K)
T	tape
T_{DP}	dew point temperature (K)
v	millivolts referenced to 0^oC
V	volume flow rate (m^3/s)
w	humidity ratio (kg/kg)
W	desiccant moisture content (kg/kg)
W	water
x'	dimensionless length

Greeks

β	ratio of nozzle diameter to duct diameter (dimensionless)
γ	property ratio analogous to the ratio of heat capacities

NOMENCLATURE (Concluded)

Γ_j	mass flow ratio of dry desiccant to air (dimensionless)
Γ_{jp}	predicted Γ_j
ΔP	differential pressure across nozzle (Pa)
ε	temperature or moisture effectiveness
ε_{Hx}	ε for heat exchanger
θ'	dimensionless time
Λ_j	number of mass transfer units for period j
Λ_{ja}	apparent Λ_j
Λ_{jp}	predicted Λ_j

1.0 INTRODUCTION

1.1 Background

Solid desiccant cooling systems have received considerable interest as a mechanically simple, solar-fired option to conventional vapor compression air-conditioning systems for HVAC applications. These systems offer potentially lower cooling costs to the consumer. They would provide the natural gas utilities with a new summer market and may help reduce peak summer air-conditioning loads on electric utilities.

Two system configurations (Figures 1-1 and 1-2) using rotary dehumidifiers are being considered for residential applications. Several studies have indicated that these systems can be competitive with vapor compression air-conditioning if thermal coefficients of performance (COP) greater than 1.2 can be obtained (Booz-Allen and Hamilton 1981; Jurinak 1982; Scholten and Morehouse 1983). Commercial and industrial applications of solid desiccant dehumidification combined with vapor compression sensible cooling are also being considered (Cohen, Levine, and Arora 1983; Howe, Beckman, and Mitchell 1983).

To make these systems economically viable researchers are trying to develop high-performance, solid desiccant dehumidifiers with low pressure drops for air-conditioning applications. The Institute of Gas Technology (IGT) investigated a corrugated passage, laminar flow matrix (Macriss and Zawacki 1982). SERI further developed a parallel-passage, laminar flow matrix (Schlepp and Barlow 1984). Exxon, with funding from the Gas Research Institute (GRI), tested a similar design that contained additional heat capacity material (Huskey et al. 1982). Table 1-1 shows the projected performance of these systems. Further information is available in Schlepp and Schultz (1984). In addition, Kang (1985) has proposed new desiccant cycle arrangements with COPs exceeding 2.5.

Commercialization of solid desiccant technologies is just beginning. American Solar King (1984) and Sharp (1982) are readying ventilation cycle systems for the residential market. ThermoElectron/GRI and Cargocaire are actively testing in the field systems that combine desiccant dehumidification with vapor compression sensible cooling (Cohen, Levine, and Arora 1983).

Developing solid desiccant dehumidifiers includes much analytical work in systems analysis and component modeling. This work has simulated seasonal system performance, estimated energy and cost savings, investigated the effects of various desiccant materials, and provided information on how to optimize performance through dehumidifier design and system operation. However, many of the models used, especially those available to the academic community and those not involved with hardware development, were not adequately verified against experimental data. The acceptance of solid desiccant cooling by the research, HVAC, and consumer communities depends on having adequate design tools for this fundamental heat and mass exchange process.

1.2 Purpose of Test Facility

The Solar Energy Research Institute's (SERI) Desiccant Cooling Cyclic Test Facility obtains test data on rotary solid desiccant dehumidifiers operated under conditions typical of

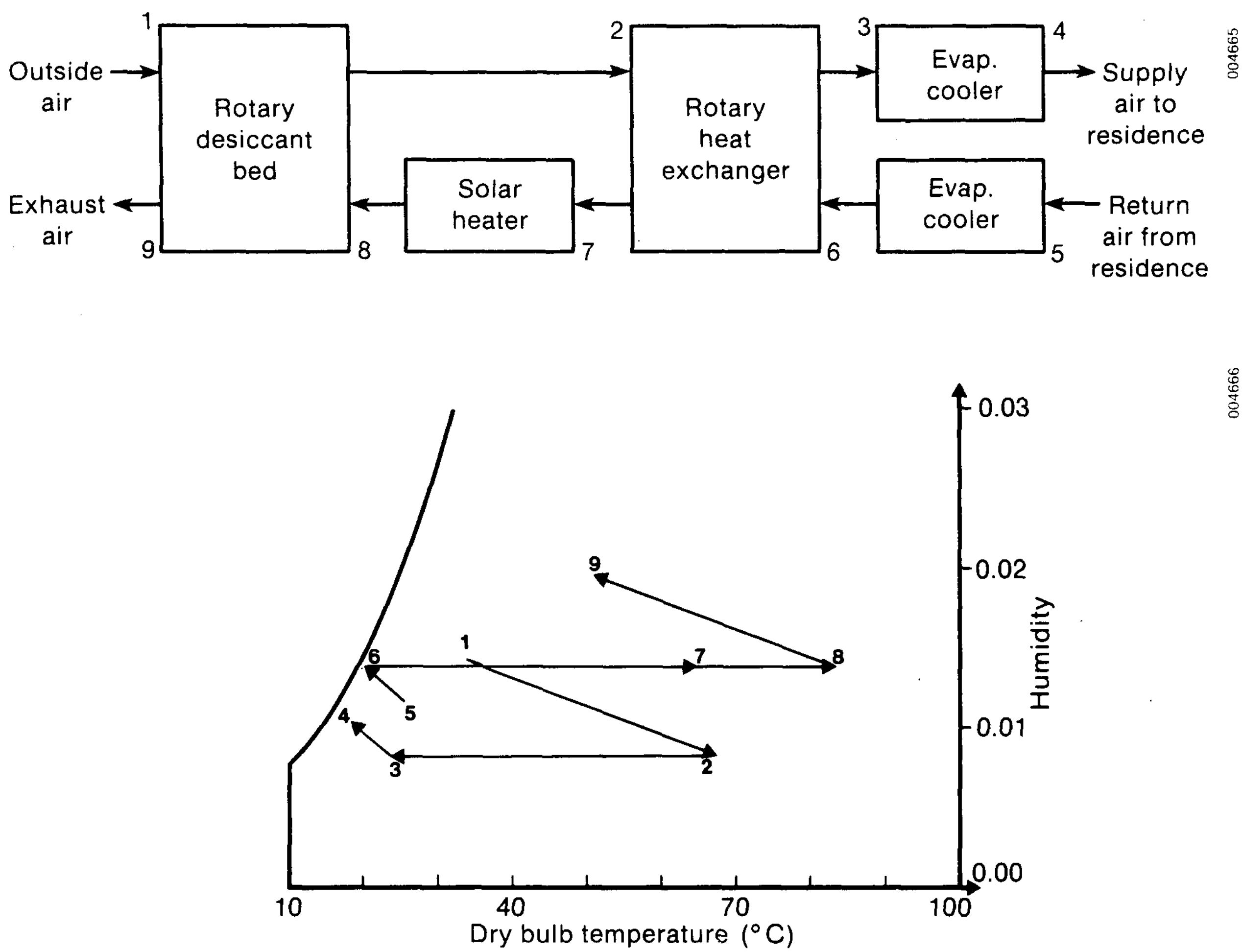

Figure 1-1. The Ventilation Cycle Desiccant Cooling System

those encountered in solar desiccant cooling applications. Several dehumidifier designs will be tested. Dehumidifier models will be checked against this data, and modifications will be made, if necessary, to ensure the models match the data. These models will then allow us to accurately simulate dehumidifier performance, optimize system operation, accurately estimate seasonal energy and cost savings, and provide useful feedback for materials and hardware development.

Two dehumidifier computer models will be compared with the data obtained: a finite difference program (MOSHMX) developed by Maclaine-cross (1974) and a simplified model (DESSIM) developed by Barlow (1982) at SERI. MOSHMX was compared with data from a rotary, packed-bed dehumidifier but with unsatisfactory results because

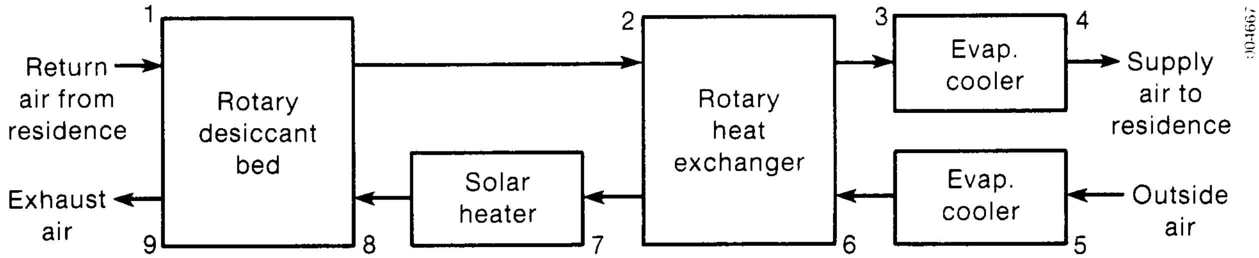

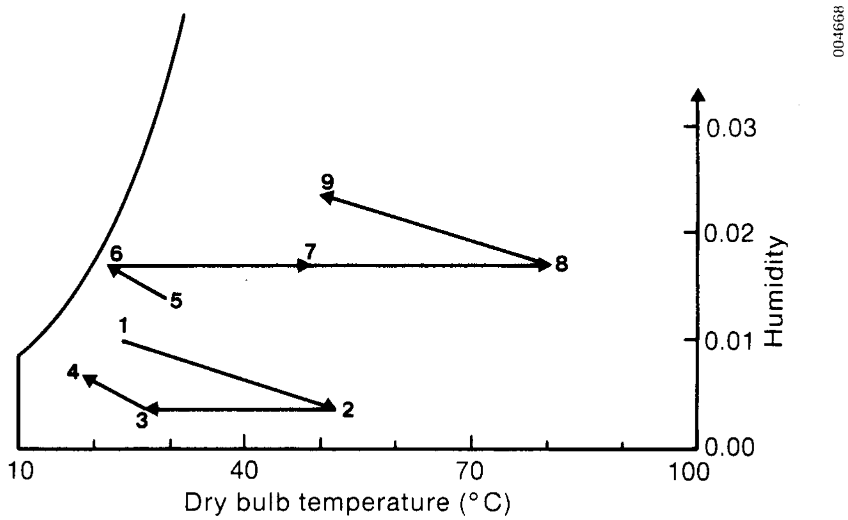

Figure 1-2. The Recirculation Cycle Desiccant Cooling System

Table 1-1. Projected Performance of Advanced Dehumidifier Systems at ARI Design Conditions

Dehumidifier	Cycle	ε_{HX}	T_{reg} (°C)	Capacity kW	Capacity kJ/kg	COP_{th}	COP_e	Type of Evaluation
IGT HCOP	Vent	0.95	--	8.4	18.7	0.95	6.2	Computer
SERI	Vent	0.95	80	--	16.7	1.07	7.2	Computer
EXXON/GRI	Vent	0.93	77	2.3	12.9	1.05	5.4	Laboratory
	Vent	0.93	77	--	15.1	1.3	8.7	Computer

of difficulties in adequately modeling the solid-side moisture transfer resistance present in the wheel (van Leersum and Close 1982); however, we expect it to work much better for high-performance designs. MOSHMX was used extensively for modeling dehumidifiers (Jurinak 1982; Brandemuehl 1982; van den Bulck 1983). DESSIM was compared with data from a single-blow experiment for both a packed bed (Kutscher and Barlow 1982) and a parallel-passage dehumidifier (Barlow 1982). It was not compared with rotary dehumidifier data, however. The data obtained from the test facility will be made available through later reports so other models can be checked.

With minor modifications the test facility can also be used for other projects, such as testing heat exchangers, evaporative coolers, and liquid desiccant system components.

2.0 DESCRIPTION OF TEST FACILITY

2.1 Overview

The test facility was designed to be flexible in characterizing the performance of dehumidifier components. The design was guided by past experience at SERI and elsewhere in building and operating similar facilities. Sources of this information outside SERI include the University of California at Los Angeles (Clark 1979), IGT (Wurm et al. 1979), Garrett AiResearch (Rousseau 1982), Illinois Institute of Technology (Monier, Worek, and Lavan 1982), Monash University/University of New South Wales (Australia) (Ambrose, Maclaine-cross, Robson 1979), Commonwealth Scientific and Industrial Research Organization (van Leersum and Close 1982; Strahm and Wilson 1982), and Exxon Corporation Energy Venture Development Group (Huskey et al. 1982). Past SERI work is documented in Kutscher and Barlow (1982) and more recently by Penney and Maclaine-cross (1985).

The initial design of the test facility is reported in Schlepp, Schultz, and Zangrando (1984). Justification for the layout, control equipment, and instrumentation chosen is given there. Several minor changes were made as the loop was put together. This report presents the current capabilities and specifications of the test loop. Use of equipment, controls, or instruments by a particular manufacturer does not constitute an endorsement of that product; any equivalent product may be used in its place.

2.2 General Layout

Figure 2-1 is a schematic of the test facility as installed in the west high bay of SERI's Field Test Laboratory Building (FTLB). The facility consists of two sections: the flow loop and the test unit. The flow loop contains all equipment and controls necessary to supply two airstreams of a given flow rate, temperature, and humidity to the test unit. The test unit consists of the test article and equipment and instrumentation to allow full testing of component performance. Figures 2-2 and 2-3 show the test facility.

2.2.1 Flow Loop Design

The flow loop has two independent streams for supplying air to the test unit at a given flow rate, temperature, and humidity. Specifications for the flow loop air states are given in Table 2-1. Figure 2-4 shows the capabilities of the test facility in relation to conditions under which a typical desiccant cooling system would operate.

At maximum flow rate a dehumidifier for an approximately 7-kW (2-ton) cooling system could be tested, assuming a cooling capacity of 15.5 kJ/kg (400 scfm/ton) could be generated (typical design values). Spiral duct of 0.3-m (12-in.) diameter and 22-gauge (0.75-mm) sheet metal was used for the flow loop. The airflow is induced by blowers powered by variable-speed motors, and electrical resistance heaters warm the air. Humidity is produced by injecting steam generated by an electric boiler. Subsequent sections of this report give details of these subsystems and their associated controls.

2.2.2 Test Unit Design

The test unit forms the framework for supporting the components to be tested, holds the instrumentation to measure the performance, and manages

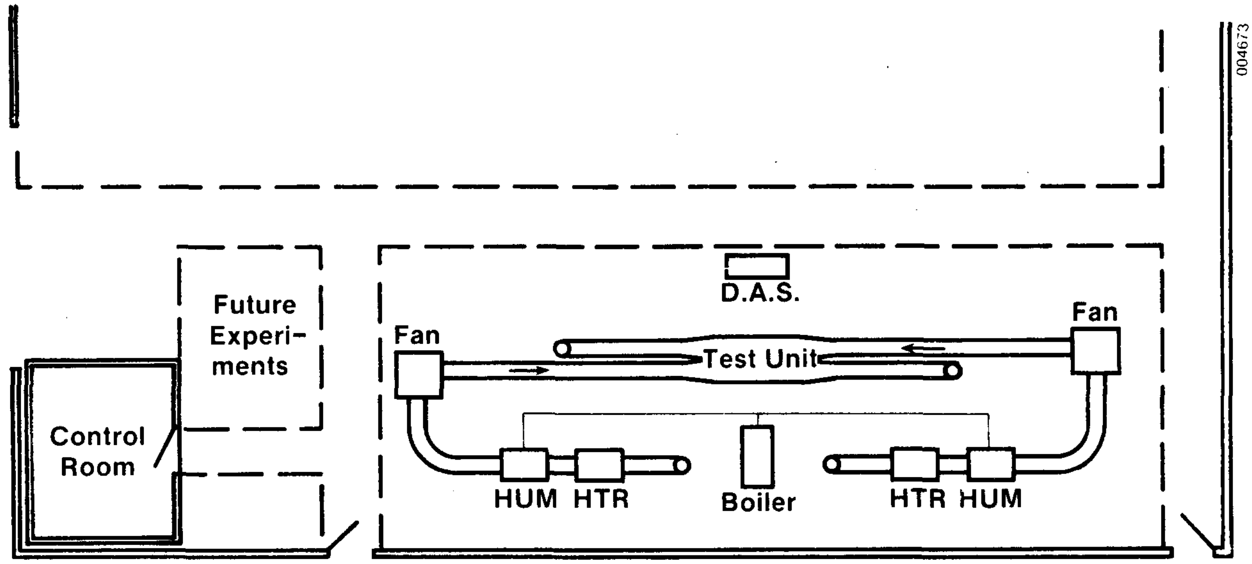

Figure 2-1. Test Facility Layout

Table 2-1. Specifications for Flow Loop Air States

Parameters	Adsorption	Regeneration
Flow rate (kg/s)	0.04-0.43	0.04-0.43
Temperature (°C)	22-40	60-90
Humidity (kg/kg)	0.008-0.020	0.008-0.020

the airflow to the components. For the current tests transition sections were fabricated to go from the round spiral duct to an approximately 0.8-m (2.5-ft) diameter half circle that matches the first test article. These sections, shown in Figure 2-5, are approximately 0.9 m (3 ft) long and were designed to expand the airflow with as little disruption as possible. However, the flow nozzle just upstream creates a rather turbulent jet of air that does not expand smoothly in the transition section. The use of screens or longer D-sections may be needed to produce uniform flow at the test article. A straight 0.3-m (1-ft), D-shaped section connects the transition section with the test article and contains the thermocouple and humidity sampling arrays for measuring the dehumidifier performance.

The sections of the duct between the inlet and outlet thermocouple locations were insulated to prevent heat losses. The regeneration stream ducting has been covered with two layers of 9-cm (3.5-in.) fiberglass bats backed with kraft paper. The process stream, because of its lower operating temperatures, was covered with only one layer.

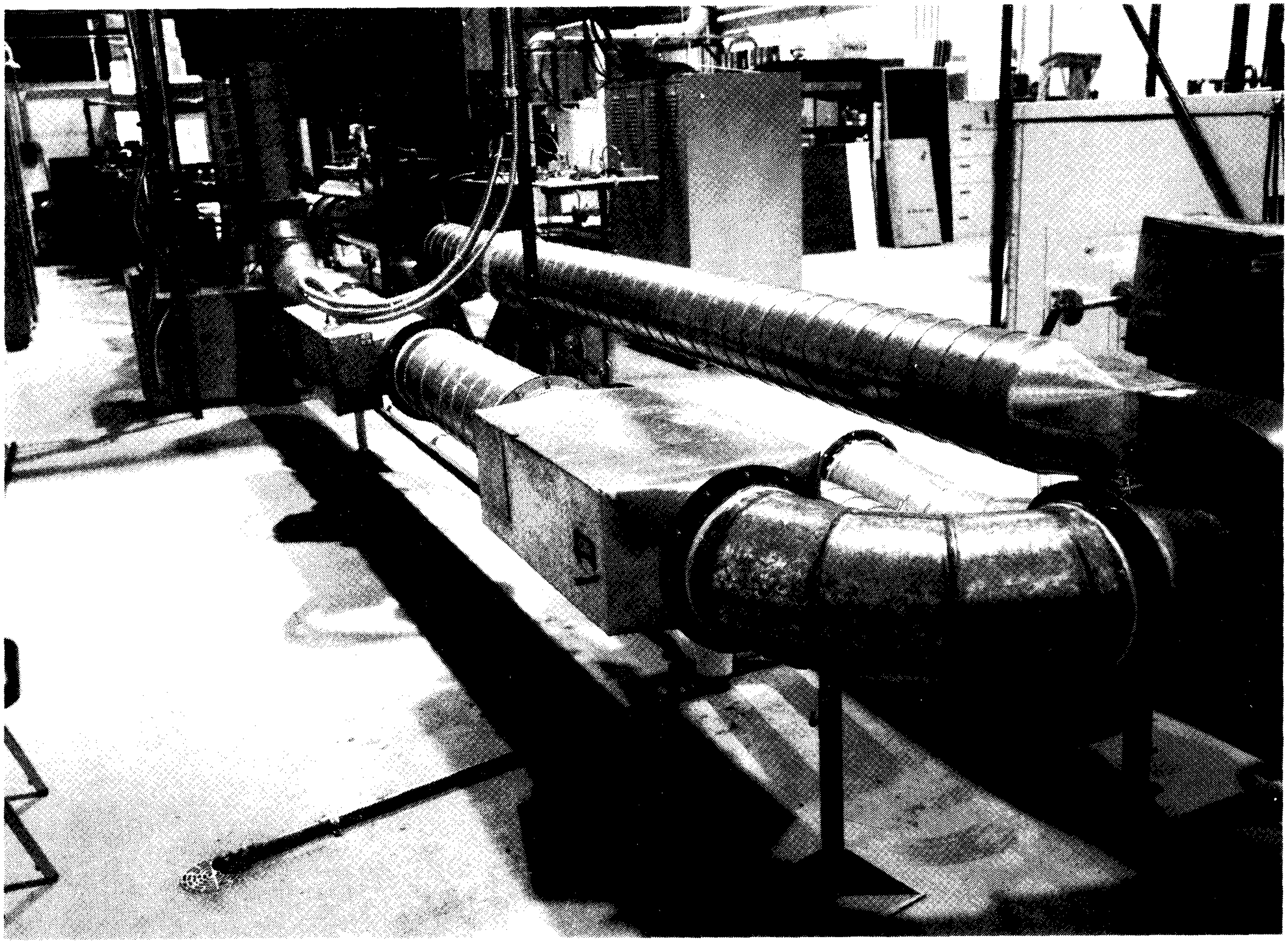

Figure 2-2. Desiccant Cyclic Test Facility Looking South to North

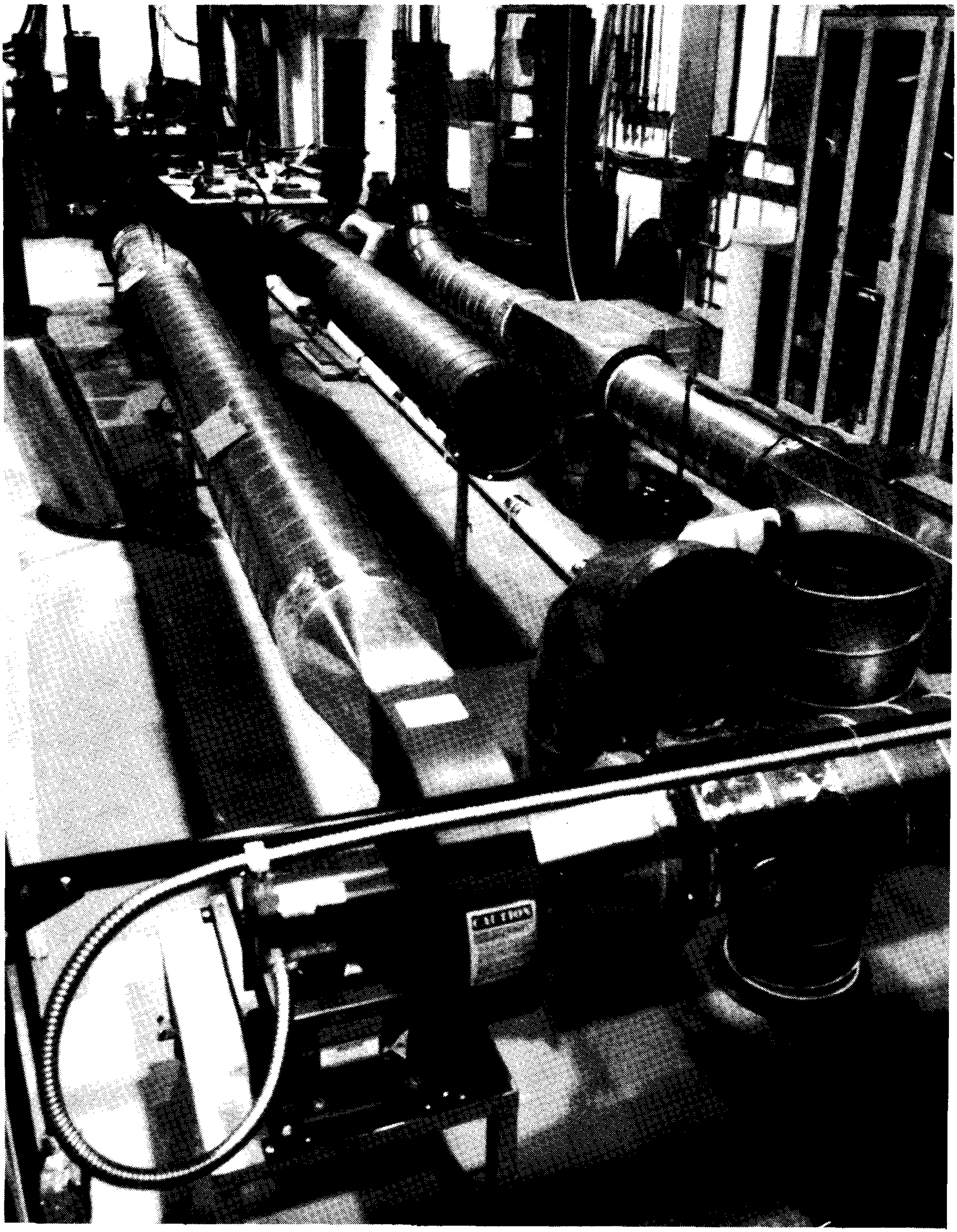

Figure 2-3. Desiccant Cyclic Test Facility Looking North to South

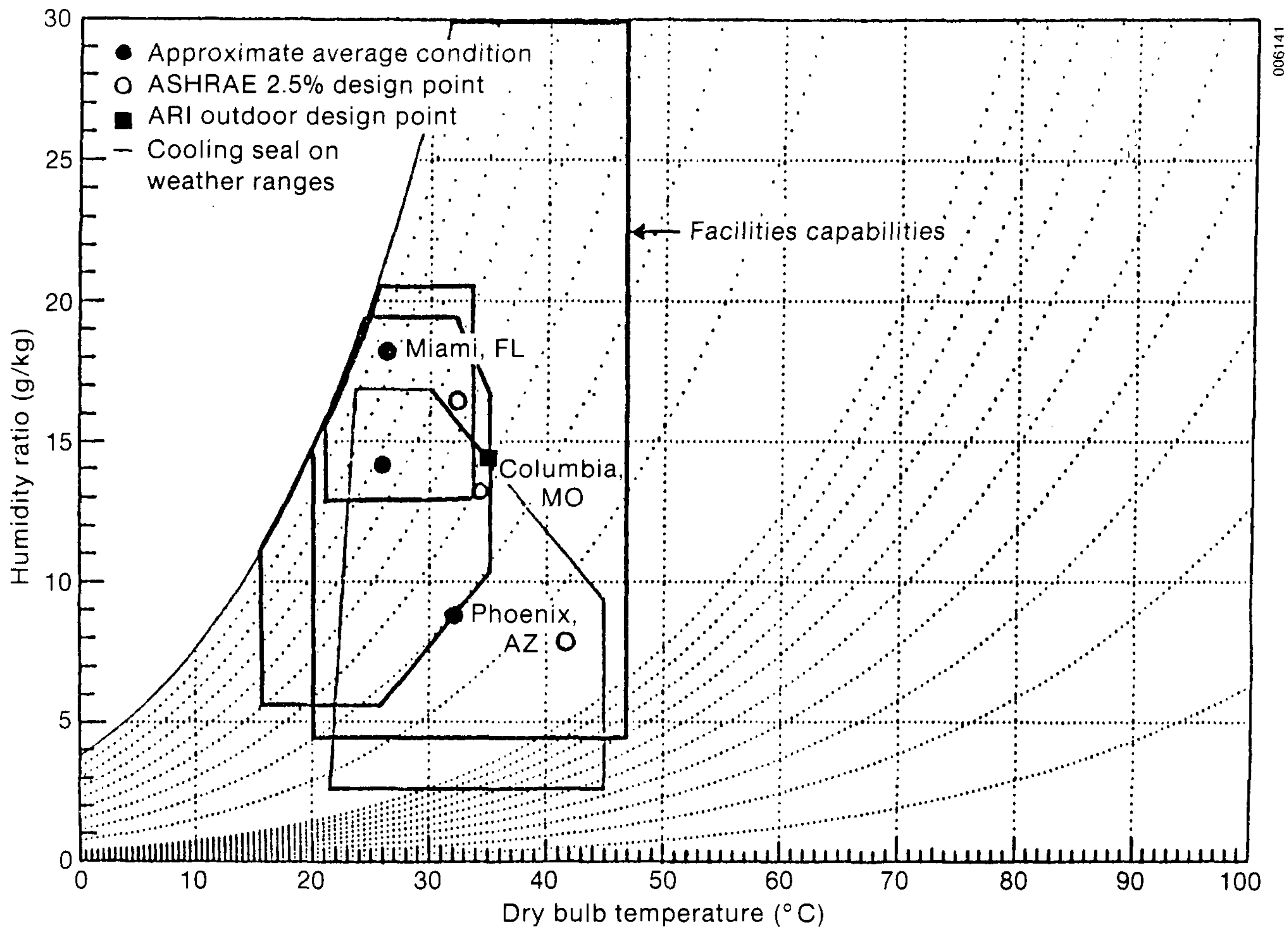

(a) Process Stream

Figure 2-4. System Capabilities

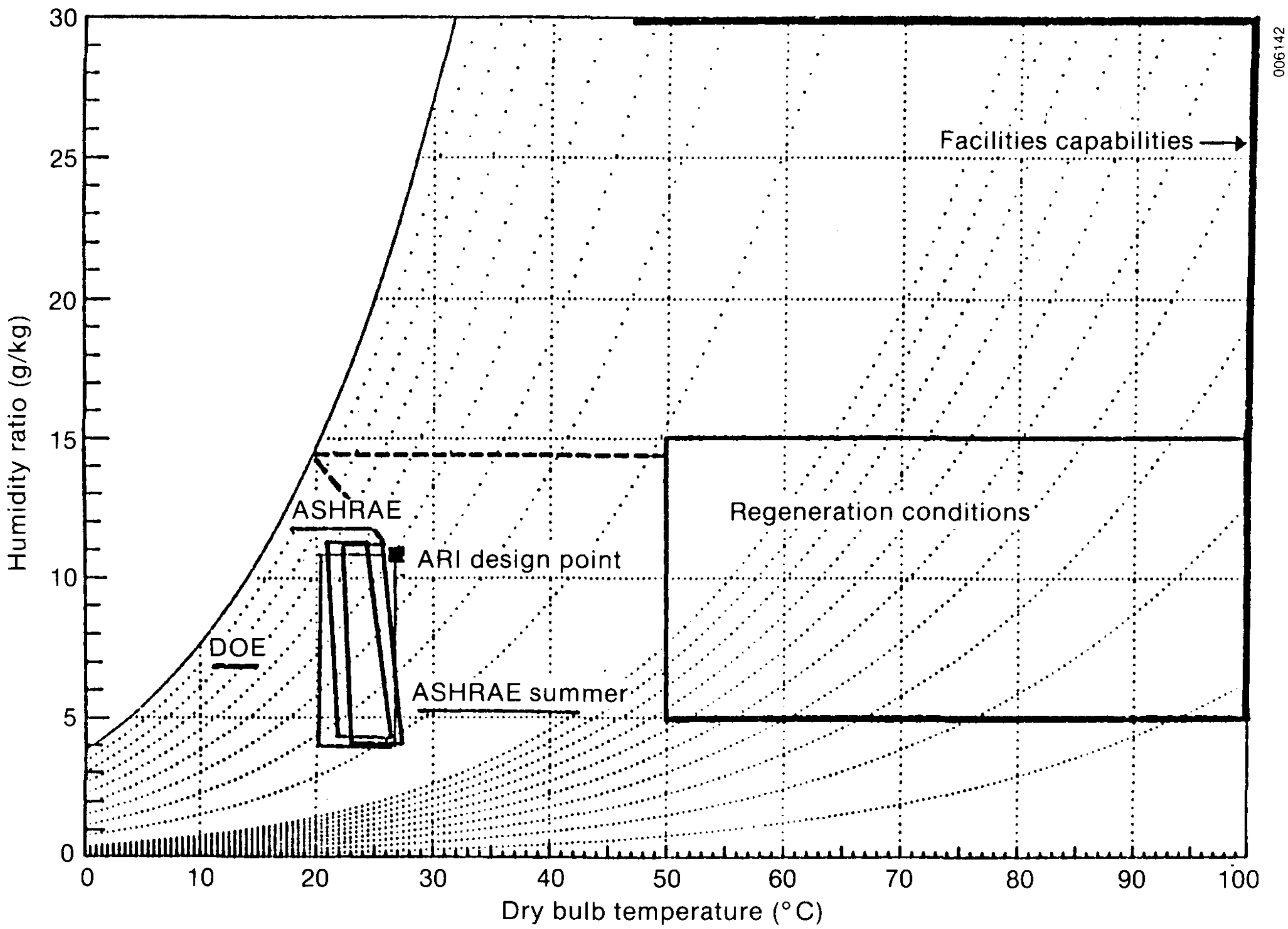

(b) Regeneration Stream (Regeneration conditions for ventilation cycle)

Figure 2-4. System Capabilities (Concluded)

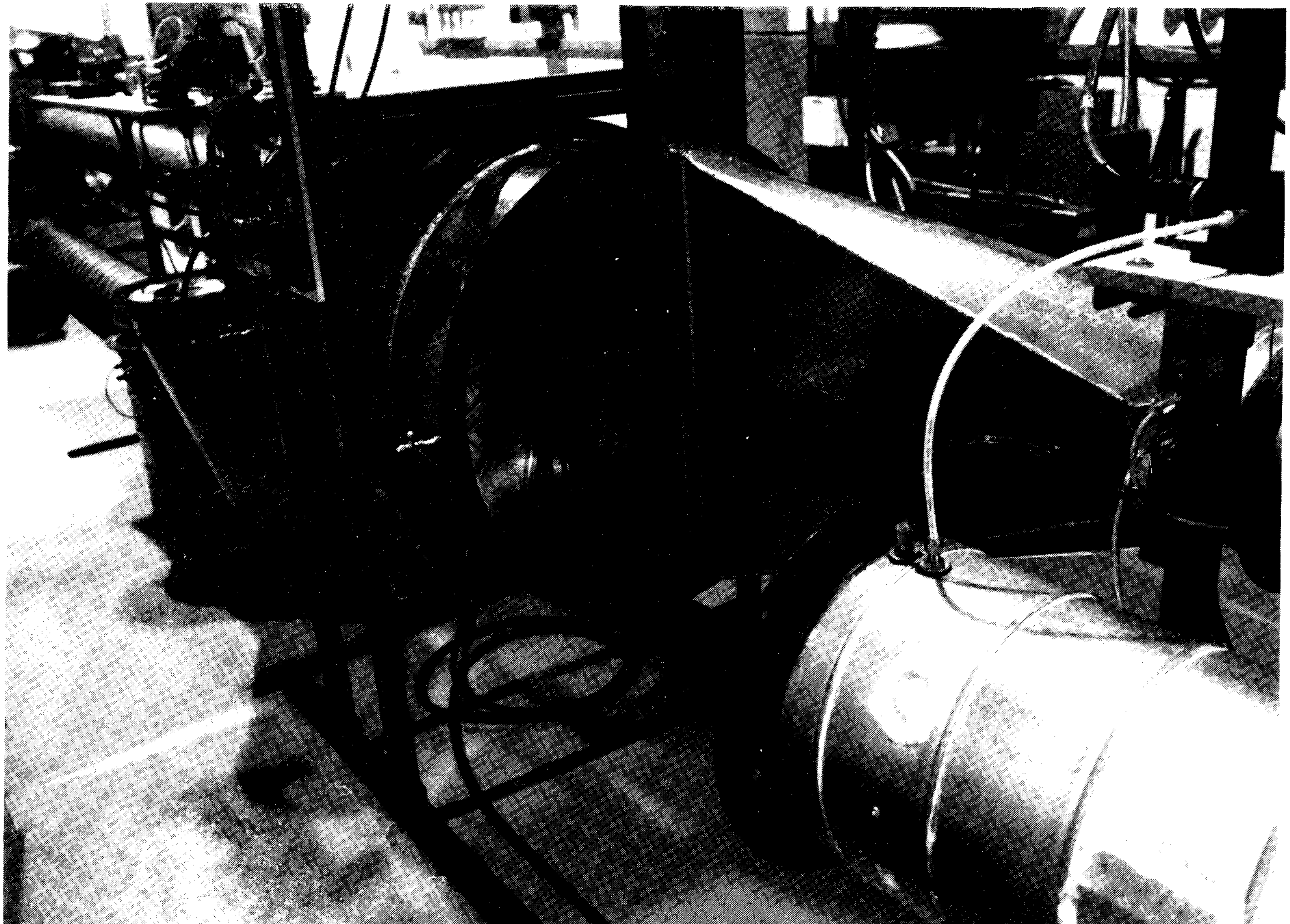

Figure 2-5. Rotary Dehumidifier in Test Facility with One Transition Section Removed

3.0 DATA ACQUISITION AND CONTROL SYSTEM

A photograph of the data aquisition and control system is shown in Figure 3-1. The center of the data aquisition and control system is a Hewlett Packard HP 3497A Data Acquisition/Control Unit. This unit contains a digital voltmeter with a 5-1/2 digit resolution and five slots for data acquisition and control cards. An extender unit (HP 3498A) provides slots for ten additional cards. Table 3-1 summarizes the cards used and the channel allocations. Voltage measurement rates are 25 readings per second with 5-1/2 digit DVM resolution and auto-zero on. This can be increased to 300 readings per second without auto-zero and use of 3-1/2 digit DVM resolution when acceptable.

An IBM personal computer (PC) with 512 kilobytes of memory and two, 360-kilobyte disk drives converts data and controls storage and the system. The IBM PC communicates with the HP 3497A over an RS-232 (serial) interface at a rate of 4800 baud. An enquire/acknowledge (ENQ/ACK) software handshake is used to coordinate the communications. Data are stored directly on diskettes and sent to a line printer. The programming language is BASIC, either interpreted or compiled. A flowchart of the program structure is shown in Figure 3-2. The transient data and control loop of the program takes approximately nine seconds when running interpreted BASIC and five seconds when running the compiled version.

Table 3-1. Data Acquisition and Control Unit Channel Allocation

Card Type (Signal)	Slots Available	Channels Available	Uses
Inputs (instrumentation)			
Voltage (with 0^{o}C ref)	3	60	Type T thermocouples
Voltage	2	40	Humidity (5 channels) Pressure (7) Wheel speed (1)
Pulse counter	2	2	Wheel speed
Outputs (controls)			
Current	3	6	Fans (variable speed motors) Heaters (silicon-controlled rectifier controllers) Humidifiers (electro-pneumatic valves)
Voltage	1	2	Wheel speed (variable-speed motor)

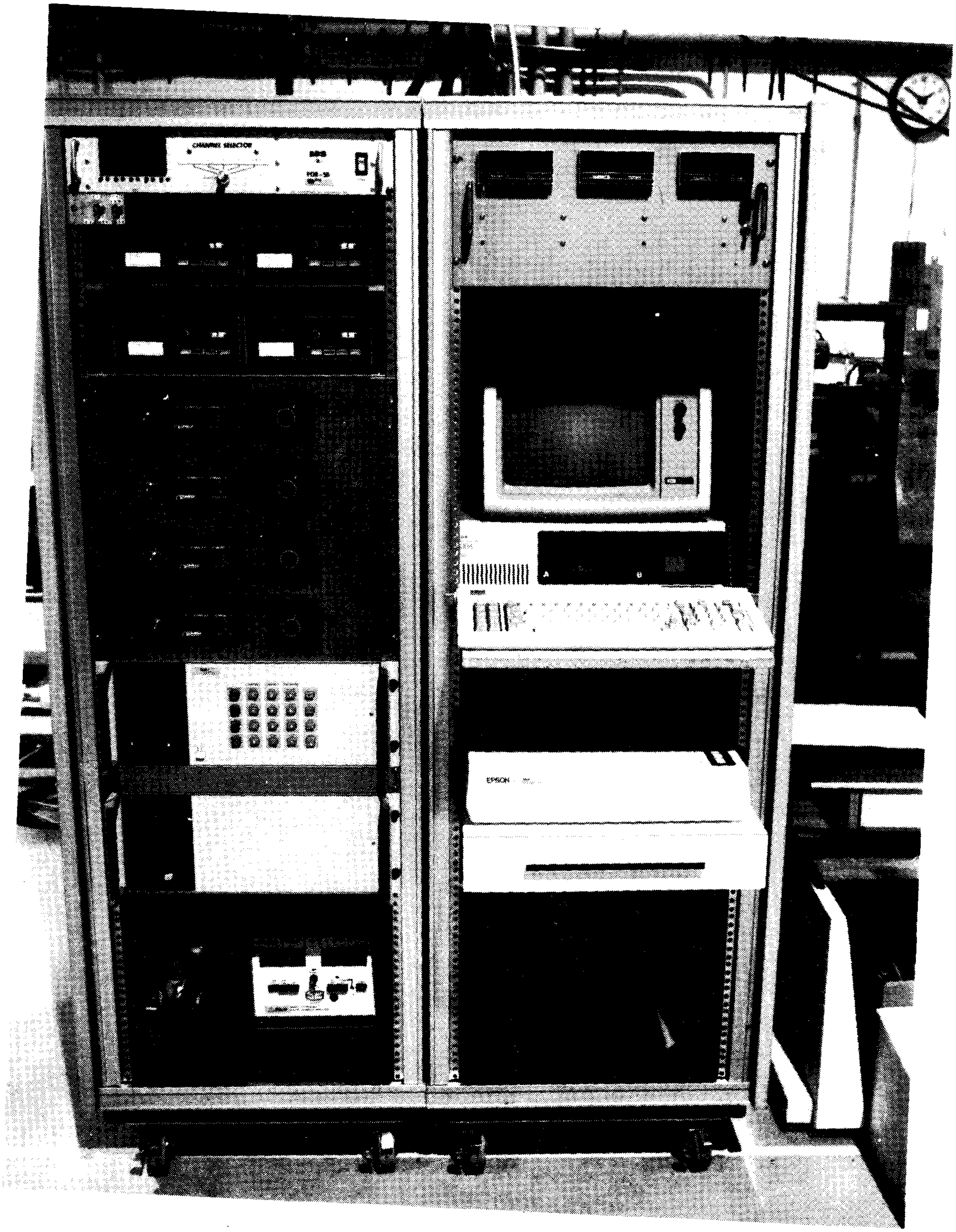

Figure 3-1. Instrumentation and Data Acquisition Center

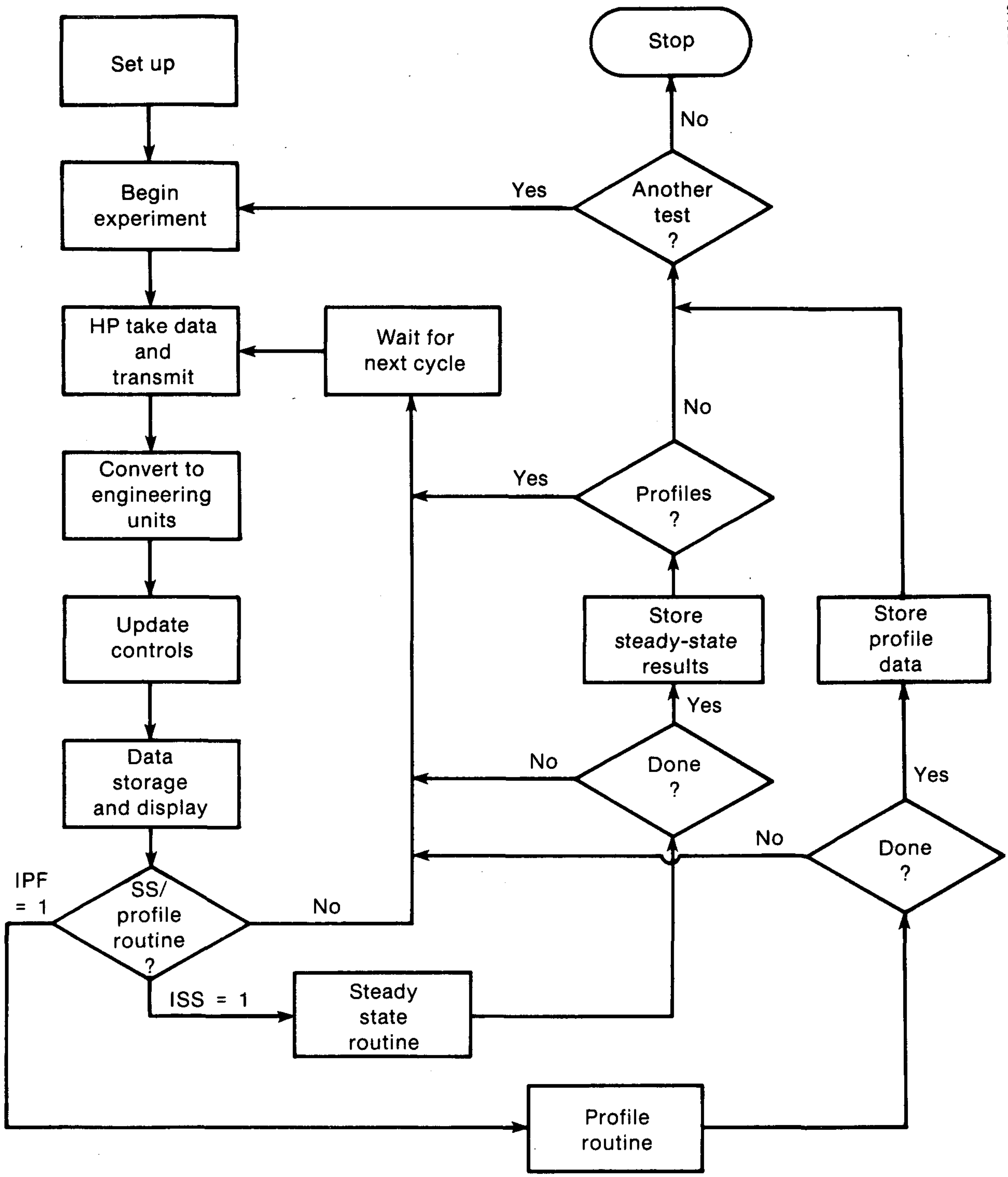

Figure 3-2. Data Acquisition Program Flowchart

4.0 CONTROLS

This section describes the equipment and equations used to control the operation of the test facility. The layout of the controls is shown schematically in Figure 4-1.

4.1 Flow Rates

Flow for each stream is produced by a blower sized to provide 0.43 kg/s at 1000 Pa, 25°C, and 0.8 atm (standard pressure at SERI's elevation, approximately 6000 ft). A performance curve is shown in Figure 4-2. The blowers are powered by 2-hp, 230-V, 3-phase motors that receive a variable frequency signal from a Fincor 5100 variable frequency speed controller (INCOM International). The controller requires a 230-V, 1-phase, 60-Hz input. The power input is converted to a DC voltage proportional to the input signal from the HP 3497A (4-20 mA, set by the computer) and then inverted into an AC voltage (3-step approximation of a sine wave) at a frequency proportional to the input reference signal. The output voltage and frequency are regulated to maintain a constant voltage-to-frequency ratio so the motor can operate at rated torque over the speed range.

For a given flow system (i.e., pressure drop versus flow rate), the volume flow rate of air produced by a fan is proportional to the fan speed. The Fincor controller produces a fan speed proportional to the input signal. The HP 3497A linearly converts

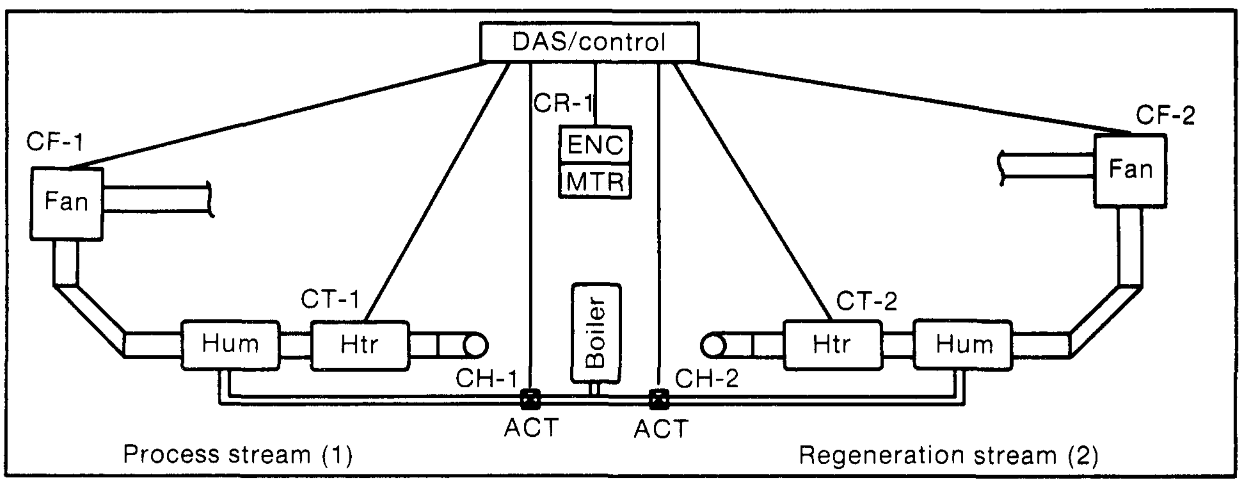

Function	Code	Range	Input (DAS)	Additional requirements
Air flow	CF-1,2	0-0.43 kg/s	4-20 mA	230 V, 1ϕ
Air temp.	CT-1 CT-2	22-40°C 60-90°C	0-12 mA 0-12 mA	
Humidity	CH-1,2	0.008-0.02 kg/kg	3-15 mA	3 atm compressed air
Rotation	CR-1	1-20 rph	0-10 V	0-5 V, TTL readout

Figure 4-1. Schematic of Control Functions and Required Ranges

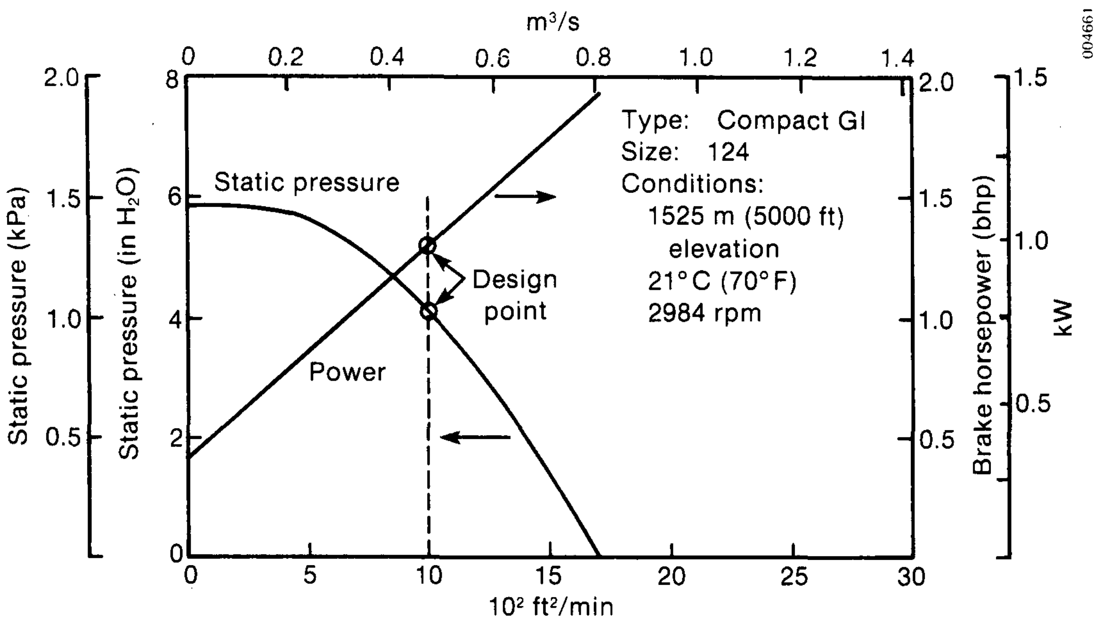

Source: New York Blower Co.

Figure 4-2. Fan Performance Curve

an integer input from the IBM PC to a current signal (0-10,000 from the PC results in a signal of 0-20 mA). Assuming we can neglect ambient pressure variations, the following equation can be written for mass flow rate:

$$\dot{m} = \frac{P}{RT} V = \frac{P}{RT} K_S K_F K_{HP}(S - S_o)$$

$$= \frac{K_f}{(273 + t)}(S - S_o) , \qquad (4\text{-}1)$$

where

$\dot{m}$ = mass flow rate (kg/s)
P = ambient pressure (Pa)
R = gas constant for air (289.6 J/kg-K)
T = absolute temperature (K)
V = volume flow rate (m^3/s)
K_S = flow system constant (m^3/s rpm)
K_F = coefficient for the Fincor controller (rpm/mA)
K_{HP} = coefficient for the HP 3497A (mA/unit)
S = integer signal from IBM PC to HP 3497A (unit)
S_o = offset signal (unit)
K_f = flow equation coefficient (kg-K/s-unit)
t = temperature (°C).

Using differential proportional control, the control equation for the mass flow rate becomes

$$S_{new} = S_{old} + G_f \frac{273 + t}{K_f} (\dot{m}_s - \dot{m}) , \qquad (4\text{-}2)$$

where

$\dot{m}_s$ = set point mass flow rate (kg/s)
G_f = gain factor, currently set to 1.0 (dimensionless).

The constant K_f is determined experimentally and must be redetermined each time the pressure drop characteristics of the system are changed (such as changing flow nozzles). Using the above equations, flow rates can be brought up to the set points in approximately 20-30 s (for a 10-s sample time) and typically can be held to within less than ±0.5%. Measuring and calculating flow rates are discussed in Section 5.4.

4.2 Temperatures

Heat is added to the airstreams through a pair of 480-V, 3-phase electric resistance duct heaters. The process stream heater has a capacity of 6 kW, and the regeneration stream heater has a capacity of 35 kW. Energy input to each heater is regulated by a silicon-controlled rectifier (SCR) controller (Halmar Electronics, series LZF2) that receives a 0- to 5-mA signal from the HP 3497A.

The temperature of the flow stream leaving the heater is given by

$$t = t_{amb} + \frac{Q}{\dot{m}c_p}$$

$$= t_{amb} + \frac{K_{SCR}K_{HP}}{\dot{m}c_p}(S - S_o)$$

$$= \frac{K_t}{\dot{m}c_p}(S - S_o) \ , \qquad (4\text{-}3)$$

where

t_{amb} = ambient temperature (^oC)
Q = energy input rate (kW)
c_p = specific heat of air (kJ/kg ^oC)
K_{SCR} = coefficient for the SCR controller (kW/mA)
K_t = temperature equation coefficient (kW/unit)
K_{HP} = coefficient for the HP 3497A (mA/unit).

Again, using differential proportional control, the control equation for temperature becomes

$$S_{new} = S_{old} + G_t\frac{\dot{m}c_p}{K_t}(t_s - t) \ , \qquad (4\text{-}4)$$

where

G_t = gain factor, currently set to 1.0
t_s = set point temperature (^oC).

The constant K_t can be determined from the characteristics of the HP 3497A output card and the SCR controllers. Power input to the heaters is monitored by an Ohio Semitronics AC watt transducer (PC 5 series). Once we approach set point conditions, we can hold the temperature to within $\pm 0.2^oC$. Temperatures can overshoot at the beginning of experiments, especially for set points much higher than ambient, because of the slow response time of the heater element and lack of insulation on the ducting between the heaters and the test unit. This problem can be reduced by manually controlling the signal from the IBM PC. Large step changes in temperature can still take 5-10 min.

4.3 Humidity

We maintained the humidity conditions by injecting steam into the airstreams. The steam is generated by an Electro-Steam, 50-kW electric boiler with on/off control through a Honeywell pressure regulator with a 1-psi (7-kPa) differential. The steam is injected into the airstream through a Walton ST-100 steam humidifier. The steam flow to each stream is regulated by a Fisher Controls electro-pneumatic valve.

Controlling the steam flow proved to be a difficult task. Maintaining a constant inlet humidity ratio is complicated by the steam pressure fluctuation in the boiler and fluctuations in the lab air humidity ratio caused by the cycling of the building air conditioning system. The control valves exhibit much hysteresis when changes in direction are called for; this has made computer control not feasible.

Currently, a relative humidity sensor (General Eastern, model 450) placed a short distance downstream of the humidifier provides a voltage signal to a differential/integral controller (Leeds and Northrup, Electromax III). The controller outputs a current signal to the control valve proportional to the difference between the sensor input voltage and the controller set point. With this setup the process stream humidity ratio can be maintained to within ±0.3 g/kg. However, the signal from the relative humidity sensor is not very sensitive to changes in humidity ratio at the low relative humidities (<5%) of the regeneration stream. Therefore, the regeneration control valve position is set manually to provide the required steam flow. Variations in regeneration inlet humidity ratio of ±0.7 g/kg are typical. This variation is caused by the boiler pressure fluctuations. Using a pressure regulator with a narrower band would help this problem. If the room humidity ratio varies significantly, the operator needs to constantly monitor the regeneration valve position.

4.4 Wheel Speed

The dehumidifier wheel is circumferentially friction-driven by a DC servomotor (Electro-Craft Corp.) turning a rubber-rimmed drive wheel through a reduction gear box (Leedy Manufacturing Co., 220:1 ratio). The DC servomotor is powered by a linear amplifier (also Electro-Craft) that outputs a voltage proportional to a ±10-V input signal from the HP 3497A. Tachometer feedback from the motor to the amplifier ensures a constant dehumidifier rotational speed to within ±0.03 rph. The ratio of the diameter of the first test article to that of the drive is 4.06:1. The maximum wheel speed for this test article is 135 rph with the above setup.

Wheel speed is highly repeatable (±0.02 rph) for a given signal from the HP 3497A; however, wheel speed varies somewhat nonlinearly (amplifier) with input signal and we could not get a reasonable regression fit. Therefore, we developed a proportional control equation to obtain accurate set point wheel speeds:

$$S_{new} = S_{old} + \frac{N_s - N}{K_w} , \qquad (4\text{-}5)$$

where

N_s = set point wheel speed (rph)
N = wheel rotation speed (rph)
K_w = wheel speed control equation coefficient (rph/unit).

The constant K_w contains the coefficient that describes the HP 3497A signal card; the amplifier and motor combination; and the speed ratios of the motor, gearbox and drive wheel, and dehumidifier wheel, and is determined experimentally by timing wheel revolutions or using a strobe light.

5.0 INSTRUMENTATION

Figure 5-1 shows schematically the measurement locations in the test loop. Table 5-1 summarizes these measurements and the instruments used. Each type of instrumentation is described further in the following sections.

5.1 Temperature

We measured temperatures using copper and constantan (type T) thermocouples. For bulk inlet and outlet temperatures we placed an array of four thermocouples connected in parallel in the duct to obtain an area weighted average. The junction design shown in Figure 5-2 provides sufficient bare wire to reduce conduction and radiation errors. The conduction error was calculated to be less than 0.01°C; the radiation error less than 0.05°C.

The profile of temperatures versus rotation angle at each dehumidifier outlet face is measured by an array of thermocouples arranged as shown in Figure 5-3. The grid is closely spaced in the region near where the dehumidifier rotates into the airstream to resolve the sharp gradient present. The more widely spaced grid over the rest of the face is sufficient for the more gentle gradients there.

To obtain the temperatures we measured the thermocouple electromotive force (EMF) with the digital voltmeter in the HP 3497A through a voltage card that provides an electronic 0°C (±0.2°C) reference temperature. The thermocouple wire was calibrated in SERI's Instrumentation/Metrology Recharge Center. The following third-order regression fit results in residuals of less than ±0.04°C over the range of 0°-100°C:

$$t = 0.0044 + 25.92v - 0.7363v^2 + 0.0402v^3 , \qquad (5\text{-}1)$$

where
t = temperature (°C)
v = millivolts referenced to 0°C.

Assuming the above noted errors combine randomly, the uncertainty in temperature measurements is less than ±0.5°C.

5.2 Humidity

Humidity measurements are made using dew point hygrometers (General Eastern, model 1100DP/1111D). These instruments have optical sensors and use chilled mirrors to control condensation. The mirror temperature is monitored by a platinum resistance thermometer and puts out a voltage signal linearly proportional to the dew point. These sensors have been calibrated by General Eastern using instruments, equipment, and standards directly traceable to the National Bureau of Standards. The stated uncertainty of the sensors is ±0.2°C. We connected the four instruments in series to simultaneously monitor the same air sample to confirm this.

We wrapped electrical heat tape around the dew point hygrometers to keep the temperature above the dew point, which prevents condensation in the tubing and sensor cavity.

Equation 5-2 converts dew point temperature to humidity ratio:

$$w = 0.622 \frac{P_{sat}(t_{DP})}{P_t - P_{sat}(t_{DP})} , \qquad (5\text{-}2)$$

where

w = humidity ratio (kg/kg)
P_{sat} = saturation pressure (Pa)

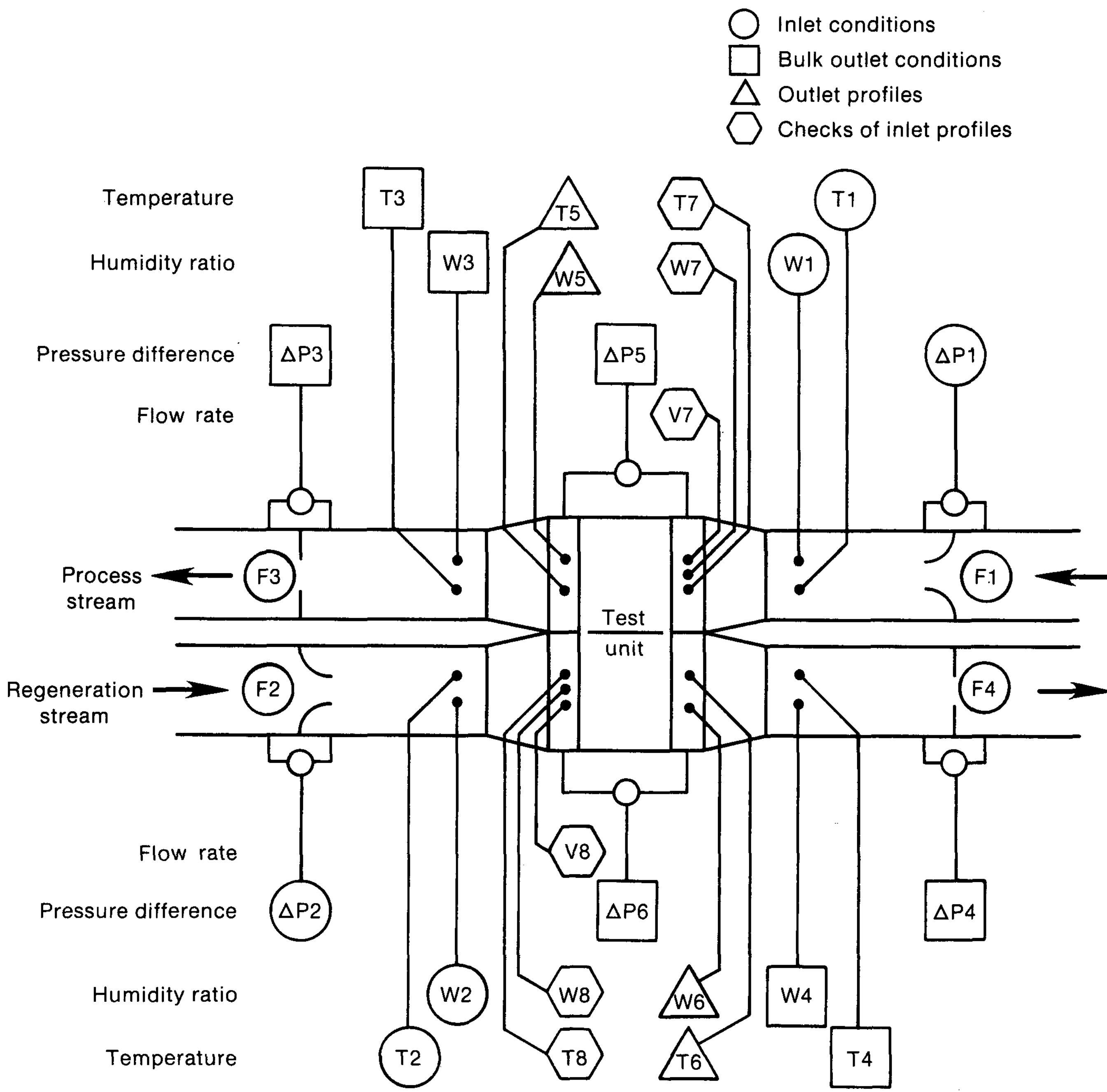

Figure 5-1. Measurement Locations (see also Table 5-1)

Table 5-1. **Summary of Required Measurements**

	Location	Figure Reference	Device	Comments
Temperatures - T				
Test run data				
	1-4	4-1	Thermocouples	Bulk conditions, inlet states are also used to control heaters
	5-6	4-1,2	Grid of thermocouples	Monitoring of outlet profiles
	9	4-3	Thermocouples	Air channel in wheel
Auxiliary data				
	7-8	4-1,2	Thermocouple probe	Inlet nonuniformities
Miscellaneous	--	--	Thermocouples	Ambient, duct walls, etc.
Humidity Ratios - W				
Test run data				
	1-4	4-1	Dew point hygrometer with fixed sample port	Bulk conditions, inlet states are also used to control boilers
	5-6	4-1,2	Dew point hygrometer with switch selectable sampling valve	Monitoring of outlet profiles
	9	5	Dew point hygrometer with internal sample port	Air channel in wheel
Auxiliary data				
	7-8	4-1,2	Dew point hygrometer movable probe	Inlet nonuniformities
Miscellaneous			Dew point hygrometer	Ambient, etc.

Table 5-1. **Summary of Required Measurements** (Concluded)

	Location	Figure Reference	Device	Comments
Flow rate - F, and associated pressure difference - ΔP				
Test run data				
	F: 1-2	4-1	Flow nozzles	Bulk inlet conditions, also used for fan control
	F: 3-4	4-1	Orifice plates	Bulk outlet conditions
	P: 1-4	4-1	Capacitance manometer	Differential
Auxiliary data				
	F: 7-8	4-1,2	Hot-wire anemometer or pilot tubes/manometer	Inlet nonuniformities
Pressure drops - ΔP (not associated with flow rate measurements)				
Test run data				
	5-6	4-1	Capacitance manometer	Differential
Miscellaneous	---	--	Capacitance manometer	Ambient - absolute system, etc. - differential

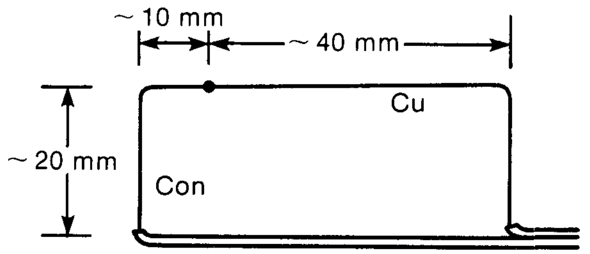

Figure 5-2. Thermocouple Design

t_{DP} = dew point temperature (^{o}C)
P_t = total absolute pressure (Pa).

Maclaine-cross (1974) developed the following correlation for saturation pressure:

$$P_{sat} = \exp\left(23.28199 - \frac{3780.82}{T_{DP}} - \frac{225{,}805}{T_{DP}^2}\right) \quad (5\text{-}3)$$

where

T_{DP} = dew point temperature (K).

The uncertainty of this correlation is less than ±0.1% (Maclaine-cross 1974). The uncertainty in humidity ratio, calculated from a Taylor series expansion and an assumption of independent errors, is less than ±2.5%.

We obtained the bulk average inlet and outlet humidity ratios by mixing air sampled across the duct cross section. The outlet humidity profiles are obtained from a grid of air sample points, shown in Figure 5-3. An electrically driven switching valve (Valco Instruments, 16 port SC type) directs each sample, in turn, to a dew point hygrometer. During steady-state operation, the outlet profile remains constant, so one instrument is sufficient for monitoring each face. This arrangement cannot adequately monitor the profiles under transient conditions.

5.3 Pressure

Pressure measurements are required for (1) pressure drop characteristics of the wheel, (2) pressure differences across the dehumidifier seals that cause leakage, (3) pressure differences across flow nozzles to calculate flow rates, and (4) ambient absolute pressure for air density and humidity ratio calculations.

Capacitance pressure sensors are used (MKS Instruments, Baratron type 221A) for differential pressure measurements and have a range of 0-10 in. of water (0-250 Pa). These sensors put out a voltage signal linearly proportional to a pressure difference. The test loop uses six sensors: two to monitor the inlet flow rates and four to monitor the pressure difference between each face of the dehumidifier wheel and the ambient air. The pressure drop through the wheel and across the radial seals separating the two flow streams are then easily calculated.

We checked the calibration of these instruments by comparing them with a Hooke gauge manometer (Dwyer Instruments, Microtector) with a resolution of ±0.0002 in. of water. The results showed a typical differential pressure error of less than ±0.5%.

Again, we use a capacitance sensor to monitor the ambient absolute pressure (MKS Instruments, Baratron type 220A). This sensor was checked against a calibrated aneroid barometer with a resolution of 0.2 torr in the SERI Instrumentation/Metrology Recharge Center. Considering temperature effects on the pressure measurement the uncertainty in the MKS instrument is less than ±0.3%.

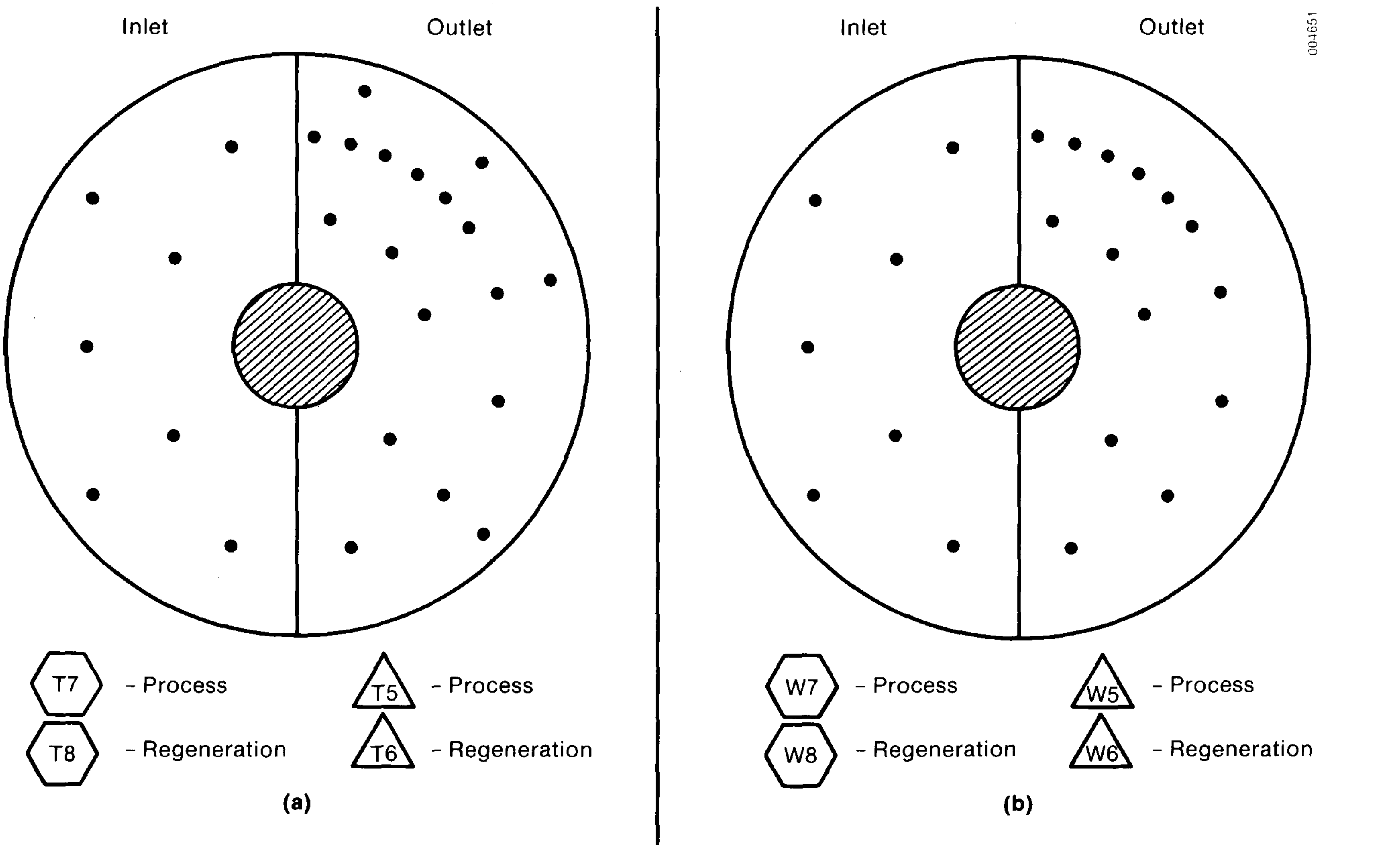

Figure 5-3. Sampling Points to Obtain Outlet Profile

5.4 Flow Rate

We obtain the flow rates by measuring the pressure difference across ASME-standard, long-radius flow nozzles. A set of nozzles will be used, ranging from 10-18 cm (4-7 in.) in diameter, to cover the range of flow rates (0.1-0.43 kg/s). We installed ten diameters of straight duct with flow straighteners upstream of the nozzle to conform to ASME standards.

Mass flow rate is calculated from

$$\dot{m} = \frac{\pi D^2}{4} \frac{C\beta^2}{(1 - \beta^4)^{1/2}} \frac{2}{R} \frac{P_t \Delta P}{(273 + t)}^{1/2}, \quad (5\text{-}4)$$

where

$\dot{m}$ = mass flow rate (kg/s)
D = duct diameter (m)
C = discharge coefficient (dimensionless)
β = ratio of nozzle diameter to duct diameter (dimensionless)
R = gas constant for air (289.6 J/kg-K)
P_t = total absolute pressure (Pa)
ΔP = differential pressure across nozzle (Pa)
t = temperature (^oC).

For a 0.305-m (12-in.) diameter duct the discharge coefficient (Bean 1971) is given by

$$C = 1.00330 - (7.920 - 2.580d^2) \times \frac{1}{(Re_d)^{1/2}}, \quad (5\text{-}5)$$

where

d = nozzle diameter (m)
Re_d = Reynolds number at the nozzle throat.

Since the uncertainty in Eq. 5-3 is larger than the variation with Reynolds number, the coefficient is calculated in the data aquisition and control program based on the set point conditions. This removes the need for an iterative solution technique. The uncertainty in discharge coefficient is given as ±2% (Bean 1971) together with the uncertainties in temperature and pressure; the uncertainty in flow rate, based on a Taylor series expansion and assumption of independent errors, is ±3.0% [see Schlepp, Schultz, and Zangrando (1984) for more details].

5.5 Wheel Speed

As discussed in Section 4.4, wheel speed is measured by monitoring the output of the feedback tachometer on the wheel drive motor. We calibrated this output versus wheel speed by timing a number of revolutions of the drive wheel and comparing them with the output. In addition, we installed an optical encoder on the wheel drive motor. It outputs two signals: a 1 pulse per revolution and a 1000 pulse per revolution square wave train. By counting pulses we can accurately measure wheel speed and easily determine the control equation coefficient K_w (Section 4.4). Repeatability of average wheel speeds is less than ±0.02 rph; variation in wheel speed with time is less than ±0.03 rph.

6.0 PRELIMINARY DATA

6.1 Description of Dehumidifier Wheel

We chose as the desiccant a spirally wound, parallel passage design using silica gel as the first test article. The design is similar to prototypes tested at SERI in the past (Schlepp and Barlow 1984) under single blow conditions. This allows us to check the test system against previous work and provides a logical basis from which to proceed to cyclic testing. The parallel-passage design was also chosen to simplify the modeling efforts since the transfer coefficients for this geometry are well-known based on theoretical and experimental work and the solid-side moisture diffusion resistance is low (Schlepp and Barlow 1984).

To construct the dehumidifier approximately 400 m of 25-μm (0.001-in.) thick polyester film with an acrylic adhesive was coated with grade 11 Davison, silica-gel particles ranging in size from 180-350 μm. This coating process is shown in Figure 6-1. We used the Davison grade 11 gel because it contained the particle sizes we needed and has an isotherm very similar to the grade 40 previously used in Schlepp and Barlow (1984). The coated tape was then sent to Rotary Heat Exchangers Pty. Ltd. of Bayswater, Victoria, Australia, for winding. Rotary Heat Exchangers uses this winding technique to produce parallel-passage heat exchangers from a 75-μm (0.003-in.) thick polyester film. Table 6-1 summarizes the dehumidifer design. Figure 6-2 shows several views of the dehumidifier.

Because of manufacturing difficulties, the windings are not as tight as desired; therefore, passage spacing is nonuniform. Although flow through the dehumidifier is fairly uniform overall, there are places where little air passes through and a lot of air passes through. This may be because of the compressibility of the desiccant-coated sheet between the spacers. The force exerted by the outer windings on the inner windings down along the spokes causes the desiccant particles to deform the tape film between the spacers as the particles from one side of the sheet fill the voids between the particles on the other side of the sheet. This compression releases the tension on the inner windings and causes sagging.

In the time available to them Rotary Heat Exchangers was unable to find an engineering solution to the compressibility problem. However, it is not the winding technique used by Rotary Heat Exchangers that is at fault but rather a limitation of the materials supplied by SERI with which they had to work with. SERI is investigating possible solutions. Basically, the recommendation is to use a smaller, more uniform desiccant particle and a stronger tape film.

In spite of these shortcomings we decided to conduct experiments on this wheel to see just how much effect the nonuniform spacing would have and also to provide a complete shakedown of the test facility.

6.2 Seal Leakage Rates

The purpose of this facility is to obtain data on the performance of a dehumidifier without concern for the physical design of the housing, seals, supports, etc. These effects will be present in the raw experimental data. However, they can be eliminated if they are known. Therefore, we measured seal leakage rates and correlated them with the appropriate pressure differences to correct the

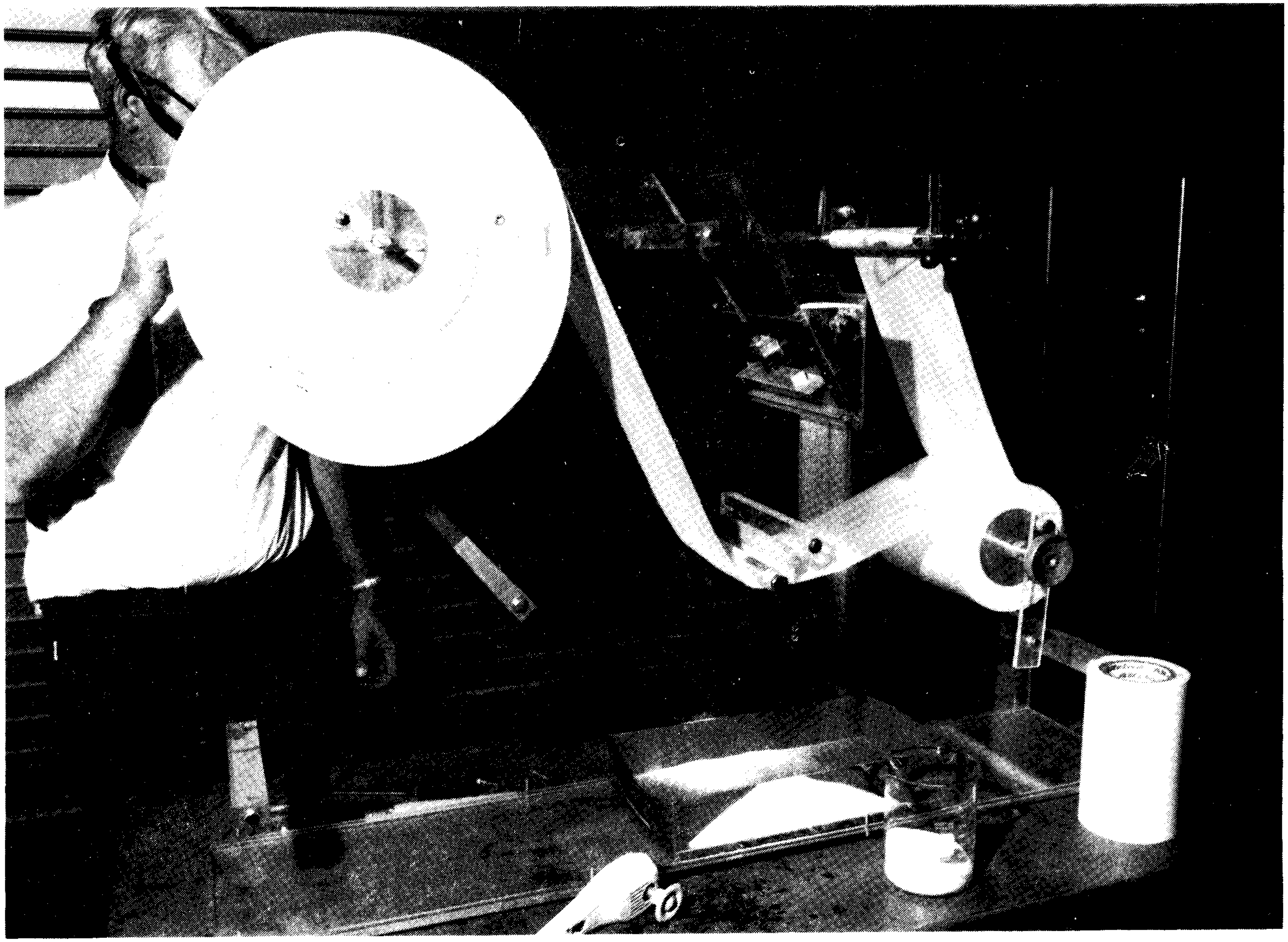

Figure 6-1. Coating of the Tape Film with Silica Gel

Table 6-1. Parameters of the First Test Dehumidifier

Outside diameter	0.8 m
Hub diameter	0.2 m
Passage depth	0.203 m
Number of spokes	16
Spacer dimensions - thickness	1.18 mm
- width	4.3 mm
Number of windings	178
Gel particle size range	180-350 μm
Sheet thickness (with gel)	0.58 mm
Passage width, average	1.04 mm
Sheet-to-sheet spacing, average	1.62 mm
Coated tape density (dry)	0.37 kg/m^2
Dry silica gel fraction	0.745
Mass of dry gel/period	7.35 kg
Mass of tape/period	2.56 kg
Face area/period	0.215 m^2

raw data. This method is based on Strahm and Wilson (1982).

A 76-μm (3-mil) polyester film attached to the spokes that contacts the center support structure, as shown in Figure 6-3a, acts as a radial seal to separate the two airstreams. The radial seal length is approximately 0.6 m on each face. The contact area is such that at least one seal is always functioning. This seal design has been used by Rotary Heat Exchangers in their rotary heat exchangers. Similar material acts as a circumferential seal, shown in Figure 6-3b, to prevent air from flowing around the dehumidifier between the rotor and the outer housing. The film is serrated to prevent the seal from buckling and to ensure contact with the rim. Figure 6-4 shows the various leakage paths in the dehumidifier, and Table 6-2 lists typical values for the leakage rates. The out leakage rate is shown for the fans upstream of the wheel. If they were downstream, ambient air would leak into the system; however, other leakages would be unaffected because the pressure differences across the seals would be similar in either case. For an inlet flow rate of 0.23 kg/s, the pressure difference through the wheel and so also across the radial and circumferential seals was approximately 68-75 Pa.

6.3 Overall Facility Operation

The test facility as described previously performed very well. Operation and control of the loop were fairly simple, although maintaining constant inlet humidity ratios was tedious, especially during the first hour or so of operation.

Closure of the dehumidifier water and energy balances, as defined by the following equations, was satisfactory:

Water balance closure:

$$\Delta W = \left[\dot{m}_{1DA}(w_1 - w_3) + \dot{m}_{2DA}(w_2 - w_4)\right] \div \left[\dot{m}_{1DA}(w_1 - w_3) + \dot{m}_{2DA}(w_2 - w_4)\right]^2 , \quad (6\text{-}1)$$

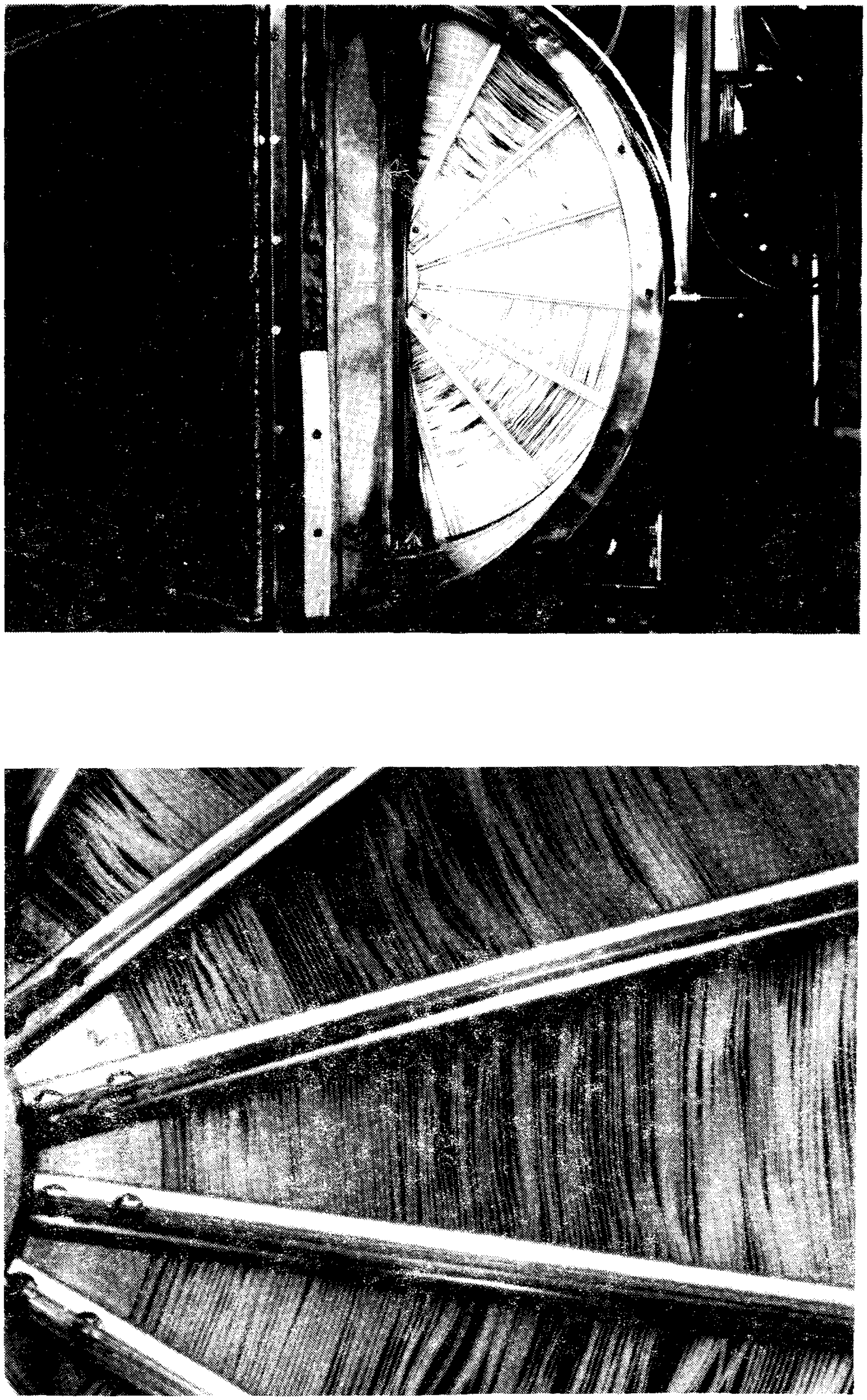

Figure 6-2. First Test Dehumidifier from Rotary Heat Exchanger, Australia

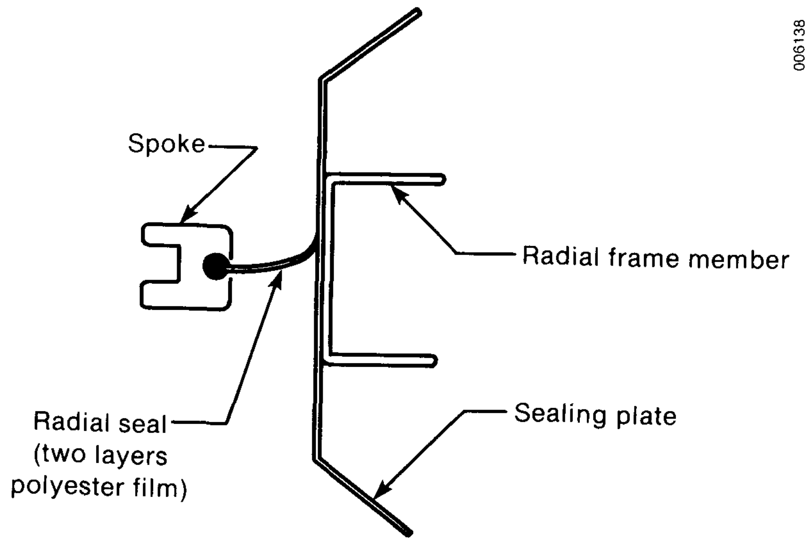

(a) Radial

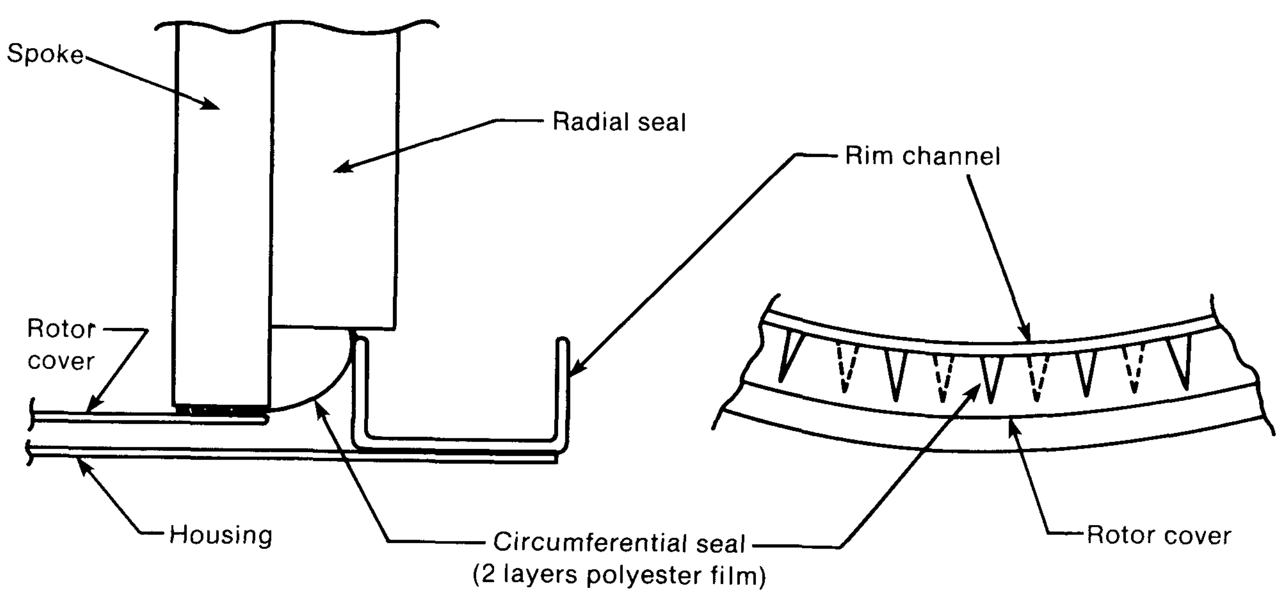

(b) Circumferential

Figure 6-3. Seal Designs

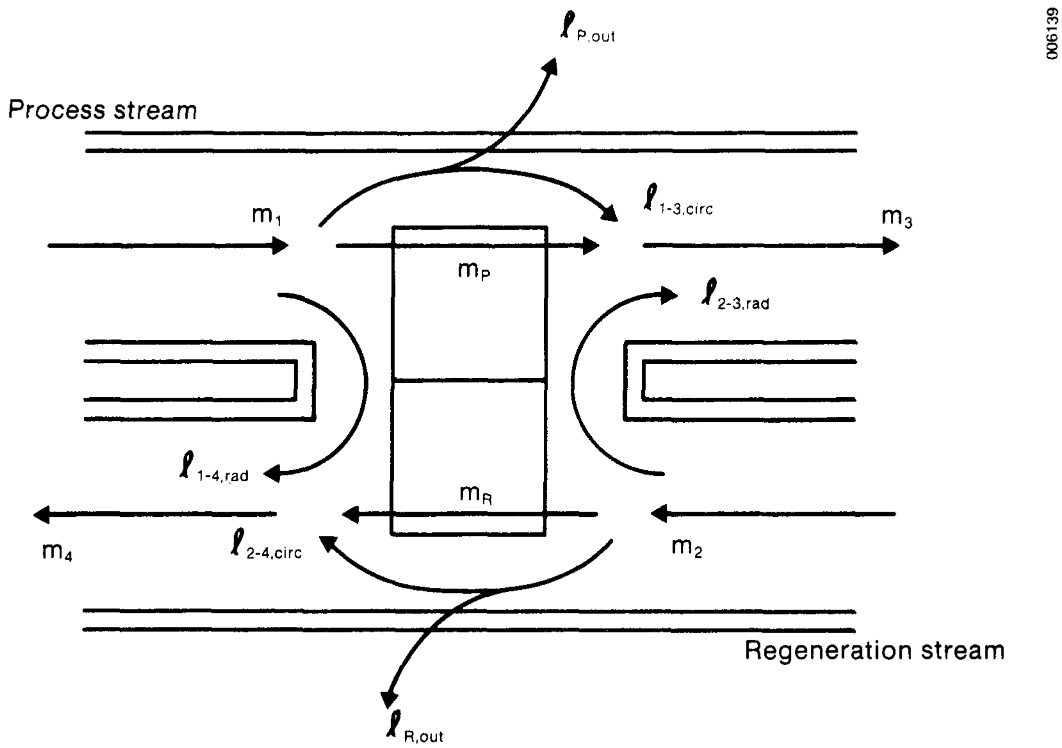

Figure 6-4. Dehumidifier Seal Leakage Paths

Table 6-2. Typical Seal Leakage Rates

Location	Percentage of Inlet Flow (%)	
	Process Stream	Regeneration Stream
Out	3.0-3.5	1.0-1.5
Circumferential	2.0-2.5	2.0-2.5
Radial	3.8-4.3	3.8-4.3

where

W = desiccant moisture content (kg/kg)
$\dot{m}_{DA}$ = flow rate of dry air (kg/s)
w = humidity ratio (kg/kg).

Energy balance closure:

$$\Delta H = \left[m_{1DA}(h_1 - h_3) + m_{2DA}(h_2 - h_4)\right) \div \left\{\left[m_{1DA}(h_1 - h_3) + m_{2DA}(h_2 - h_4)\right]/2\right\} \qquad (6\text{-}2)$$

where

h = specific enthalpy of moist air (J/kg dry air).

The state points are numbered as in Figure 5-1. Values for ΔW are typically less than ±3% with maximums of ±5%. Values for ΔH are somewhat higher because of small differences between large numbers since the dehumidification process results in small air enthalpy changes. Similar results hold for the overall test rig.

This is satisfactory for the present test article; however, improvements will be needed for testing higher performance wheels.

6.4 Initial Tests

Initial tests included several single-blow tests in an attempt to match previously taken data by Schlepp and Barlow (1984). Because of slight differences in geometry, we could not exactly match the transfer units and desiccant-to-air ratio. However, the single-blow data obtained matched the previous data well enough to indicate that the test facility and the wheel were performing satisfactorily. Also, we ran several cyclic tests to check full operation of the rig and wheel, again obtaining satisfactory results. These data are not presented here because the rig was not insulated at the time and, therefore, the energy balances did not close.

After installing needed insulation, we conducted two sets of tests to determine several important parameters of the wheel. A set of very low rotation speed tests was performed to determine how much of the silica gel in the wheel is actually active. A set of very high rotation speed tests was performed to determine the effective Lewis number (ratio of the heat transfer coefficient to the mass transfer coefficient) of the wheel.

Two parameters that describe the dehumidifier and that are used in the following analyses are the capacity rate ratio for period j, Γ_j, and the number of mass transfer units for period j, Λ_j. These are defined further in Jurinak (1982); Maclaine-cross (1974); Maclaine-cross and Banks (1972); Schlepp, Schultz, and Zangrando (1984); and Schultz and Schlepp (1984). For a particular wheel these parameters become simple functions of air flow rate and wheel rotation speed. For the first test dehumidifier these parameters are calculated as

$$\Lambda_{jp} = \frac{4.63}{m_{DAj}}$$

(Nu = 7.5 parallel-passage, laminar) (6-3)

$$\Gamma_{jp} = 0.00408\frac{N}{m_{DAj}} , \qquad (6-4)$$

where

m_{DAj} = mass flow rate of dry air in period j (kg/s)
N = wheel rotation speed (rph)
p = indicates calculation is based on physical measurements,

and where the constants 4.63 and 0.00408 were determined from the physical design of the wheel.

6.4.1 Low-Speed Tests

At very low rotation speeds the wheel comes to equilibrium with the inlet airstream before it rotates into the next period. Each differential slice of the wheel essentially goes through a complete single-blow test. The method of analysis used here transforms the coupled heat and mass transfer processes in the dehumidifier into approximately uncoupled processes, each analogous to heat transfer alone, which are then superimposed (Jurinak 1982; Maclaine-cross 1974; Maclaine-cross and Banks 1972).

With appropriate assumptions that hold fairly well for high-performance dehumidifiers the governing equations for heat and mass transfer in the dehumidifier can be transformed into a set of equations in terms of two potentials, F_1 and F_2. These potentials are similar to air enthalpy and relative humidity lines on a psychrometric chart. The transformed equations, which have the same form as the equation for heat transfer alone, are as follows (Jurinak 1982;

Maclaine-cross 1974; Maclaine-cross and Banks 1972),

$$\frac{\partial F_{ij}}{\partial \theta'} + \frac{1}{C_{ij}} \cdot \frac{\partial F_{ij}}{\partial x'} = 0 \quad i,j = 1,2 \ , \qquad (6\text{-}5)$$

where

F_i = potential 1 or potential 2
j = period 1 (process) or period 2 (regeneration)
θ' = dimensionless time
x' = dimensionless length

and

$$C_{ij} = \gamma_{ij}\Gamma_j = \gamma_{ij}\frac{m_{DD}N}{\dot{m}_{DA}} \ , \qquad (6\text{-}6)$$

where

C_{ij} = reciprocal of the dimensionless wave speed for potential i in period j
γ = property ratio analogous to the ratio of heat capacities
m_{DD} = mass of dry gel (kg)
$\dot{m}_{DA}$ = flow rate of dry air (kg/s).

Because of the values of γ, the F_2 wave moves through the wheel much more slowly than the F_1 wave does. At low rotation speeds, defined as

$$\frac{1}{C_{2j}} >> 1 \text{ or } C_{2j} << 1 \ , \qquad (6\text{-}7)$$

the F_2 wave moves completely through the wheel before it rotates into the next period. An F_2 effectiveness η_{2j} can be defined analogously to the heat transfer effectiveness and it can be shown that

$$\eta_{2j} = C_{2j} \qquad (6\text{-}8)$$

for very low rotation speeds (Maclaine-cross 1974; Maclaine-cross and Banks 1972). We can calculate η_{2j} from test data using the following equations:

where the state points are as shown in Figure 6-5. Assuming that the properties of the gel/matrix combination are known, test data at very low rotation speeds would provide a check on the amount of active dry gel m_{DDa} in the dehumidifier. The silica gel and matrix properties used are given in Table 6-3.

To perform this check the five tests listed in Table 6-4 were run and analyzed with the above method. The outlet states of each test are shown in Figure 6-5. Note that as the rotation speed increases, the outlet states move toward the intersection point of the F_i characteristics. As the wheel speed increases, more air is processed by the wheel and less comes through unaffected.

The F_2 effectivenesses are plotted against C_{2jp} calculated from physical measurements in Figure 6-6. Note that the slope of the line deviates from unity even at very low C_{2jp}. A linear least squares fit through zero and the results of tests LS-1A and LS-2A, shown in Figure 6-7, give a slope of 0.903. This indicates that the active amount of silica gel in the matrix is approximately 90% of that calculated to be there, or

$$\frac{m_{DDa}}{m_{DDp}} = 0.903 \ , \qquad (6\text{-}11)$$

where the subscript a refers to the active value and the subscript p refers to the physical value. This could be a result of the tape adhesive blocking some of the silica gel pores and reducing the gel's water holding capacity. Future sorption equilibrium tests at SERI on the tape

$$\eta_{21} = \frac{(t_3 - t_1)(w_2 - w_{31P}) - (w_3 - w_1)(t_2 - t_{31P})}{(t_{31P} - t_1)(w_2 - w_{31P}) - (w_{31P} - w_1)(t_2 - t_{31P})} \ , \qquad (6\text{-}9)$$

and

$$\eta_{22} = \frac{(t_4 - t_2)(w_1 - w_{41P}) - (w_4 - w_2)(t_1 - t_{41P})}{(t_{41P} - t_2)(w_1 - w_{41P}) - (w_{41P} - w_2)(t_1 - t_{41P})} \ , \qquad (6\text{-}10)$$

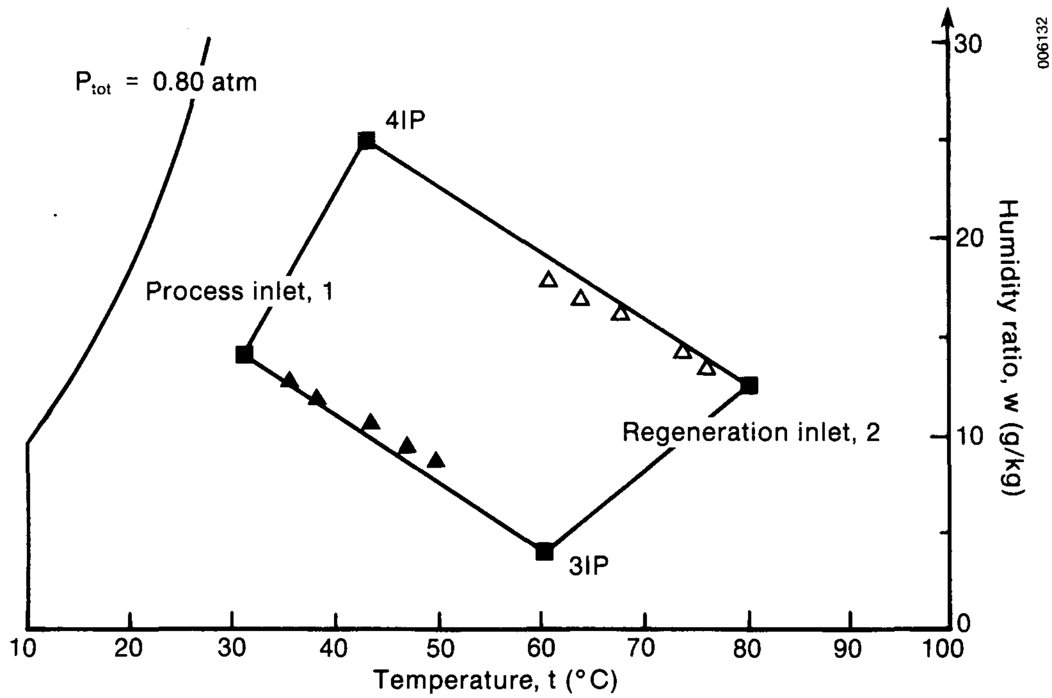

Figure 6-5. Low Rotation Speed Outlet States

Table 6-3. Silica Gel and Matrix Properties

Equilibrium relationship (Brandemuehl 1982)

$$P_v = \frac{1}{29.91}[(29.91)(2.112W)P_{sat}]^{h_s/h_v} ,$$

where

P_v = equilibrium vapor pressure (atm)
P_{sat} = saturation vapor pressure (atm)
W = desiccant moisture content (kg/kg).

Heat of adsorption (Brandemuehl 1982)

$$h_s/h_v = 1 + 0.2843e^{-10.28W} ,$$

where

h_s = heat of adsorption
h_v = latent heat of vaporization of water.

Specific heat of silica gel (Schlepp and Barlow 1984) = 921 J/kg °C

Specific heat of tape (Schlepp and Barlow 1984) = 1840 J/kg °C

Table 6-4. Low-Rotation Speed Tests

Average inlet conditions

$m_1 = 0.208\ kg_{DA}/s$ $m_2 = 0.214\ kg_{DA}/s$

$t_1 = 31.0^oC$ $t_2 = 80.0\ C$

$w_1 = 14.0\ g/kg$ $w_2 = 12.5\ g/kg$

Intersection points

$t_{31P} = 60.4^oC$ $t_{41P} = 42.7^oC$

$w_{31P} = 4.0\ g/kg$ $w_{41P} = 24.8\ g/kg$

Average γs

$\gamma_{21} = 23.7$ $\gamma_{22} = 16.7$

Outlet states

Test No.	t_3 (°C)	w_3 (g/kg)	t_4 (°C)	w_4 (g/kg)	N (r/h)
LS-1A	35.3	12.60	75.8	13.34	0.335
LS-2A	38.2	11.74	73.5	14.14	0.567
LS-3A	43.3	10.37	67.6	15.84	1.179
LS-4A	46.9	9.24	63.3	16.67	1.782
LS-5A	49.6	8.58	60.7	17.68	2.399

Effectivenesses

Test No.	η_{21}	η_{22}	C_{21P}	C_{22P}	C_{21a}	C_{22a}
LS-1A	0.1446	0.1006	0.1557	0.1068	0.1406	0.0964
LS-2A	0.2369	0.1630	0.2634	0.1808	0.2379	0.1633
LS-3A	0.3940	0.3165	0.5478	0.3760	0.4947	0.3395
LS-4A	0.5122	0.4127	0.8280	0.5684	0.7477	0.5133
LS-5A	0.5941	0.4908	1.1147	0.7652	1.0066	0.6910

and gel combination may answer the latter question.

Shown in Figure 6-8 is the expected theoretical results for F_2 effectiveness. The deviation appears to be because of a reduced number of transfer units. Based on the physical dimensions of the wheel, the NTUs are calculated to be

$$\Lambda_{jp} = 22 \text{ or } NTU_o = 11 ,$$

where

Λ_{jp} = predicted number of mass transfer units for period j

NTU_o = overall number of transfer units.

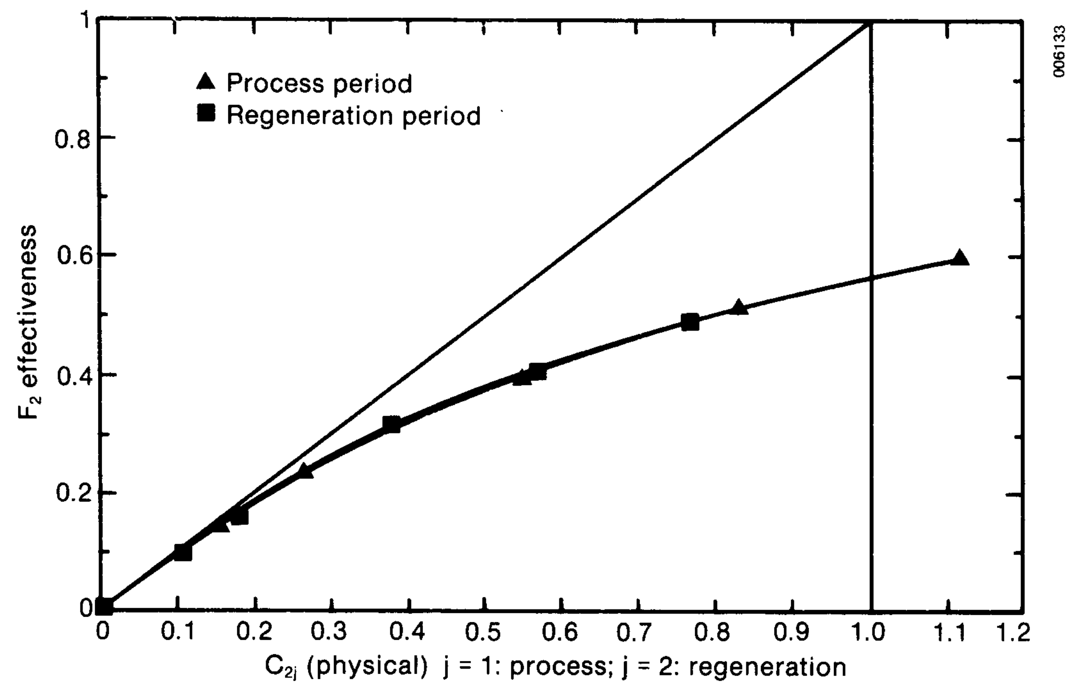

Figure 6-6. F_2 Effectiveness versus C_{2jp}

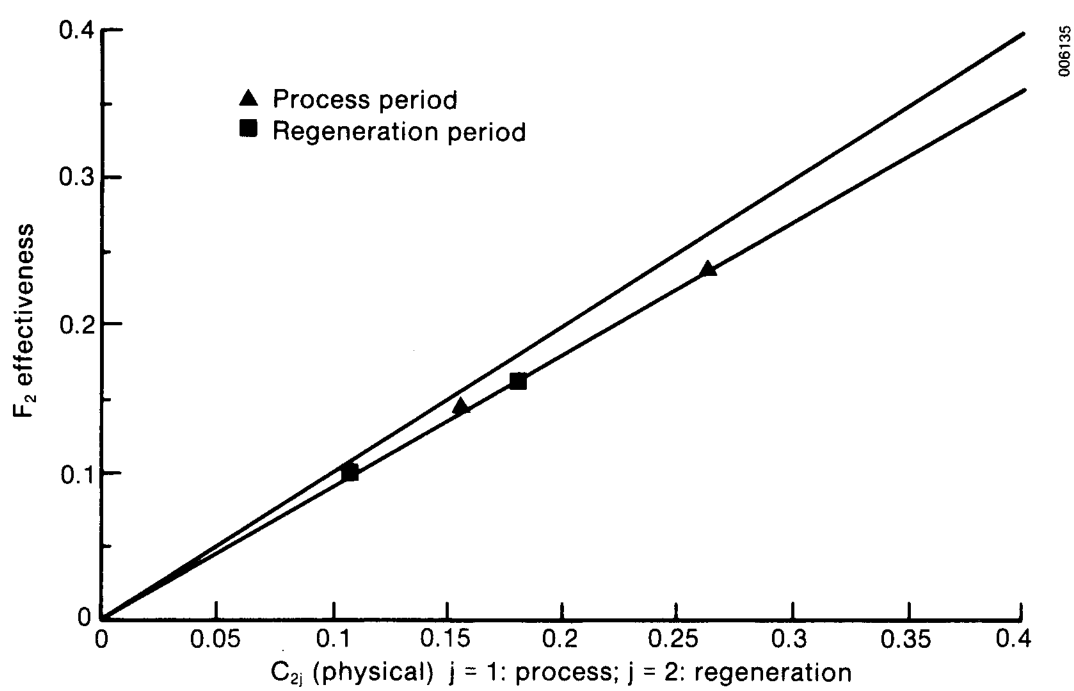

Figure 6-7. Fit to Very Low Speed Data

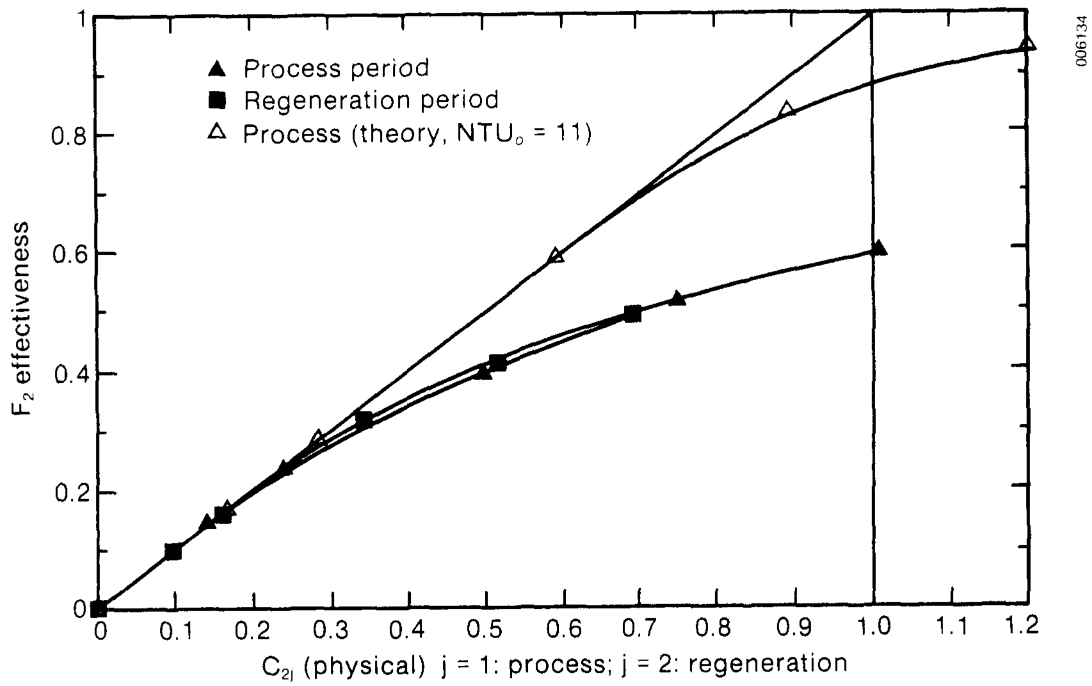

Figure 6-8. F_2 Effectivess versus C_{2ja}

The apparent values from the data appear to be

Λ_{ja} = 6 to 8 or NTU_o = 3 to 4 ,

where

Λ_{ja} = apparent number of mass transfer units for period j.

This result is discussed further in Section 7.0.

6.4.2 High-Speed Tests

At very high rotation speeds the dehumidifier acts as a total enthalpy exchanger. The outlet of one stream approaches the inlet of the opposite stream. In terms of the analogy method the fast moving F_1 wave does not have time to move completely through the wheel,

$$\frac{1}{C_{1ja}} \ll 1 \text{ or } C_{1ja} \gg 1 .$$

If the inlet conditions have the same humidity ratio, the wheel will then seem to act as a temperature exchanger. From an experimentally obtained temperature effectiveness we can determine the overall number of transfer units for heat transfer NTU_{to} (Maclaine-cross and Banks 1972; Kays and London 1964). If the inlet conditions have the same temperature but different humidity ratios, the wheel acts as a mass exchanger. As with temperature, we can determine the overall number of transfer units for moisture transfer NTU_{wo}. The ratio of these values is the Lewis number,

$$Le_o = \frac{NTU_{to}}{NTU_{wo}} .$$

Using the notation of Kays and London (1964),

$$NTU_o = fn(\varepsilon, C^*, C_r^*) , \qquad (6\text{-}12)$$

where

ε = temperature or moisture effectiveness
$C^* = C_{min}/C_{max}$
$C_r^* = C_r/C_{min}$

and

$$C \begin{cases} = \dot{m}_{DA}c_{pA} & \text{for heat transfer} \\ = \dot{m}_{DA} & \text{for mass transfer} \end{cases}$$

$$C_r \begin{cases} = [m_{DDa}(c_{pDD} + Wc_{pW}) + m_T c_{pT}]N \\ \quad \text{for heat transfer} \qquad (6\text{-}13) \\ = m_{DDa}N \text{ for mass transfer,} \end{cases}$$

where

A = moist air
DA = dry air
DD = dry desiccant
T = tape
W = water.

Table 6-5 lists the tests we ran to check the Lewis number of the first test dehumidifier. The state points are shown on a psychrometric chart in Figure 6-9. The results show that the wheel exhibits a Lewis number near unity. Based on period 2 results, the Lewis number could be as high as 2. This variation is a result of uncertainties in the mass and energy balance closures.

Again, as for the low speed tests, the experimentally determined NTUs are about a factor of 3-4 less than was expected based on the physical dimensions of the wheel. For set A it was

$$\Lambda_{jp} = 22 \text{ or } NTU_o = 11 \ ,$$

and for set B,

$$\Lambda_{jp} = 30 \text{ or } NTU_o = 15 \ .$$

This is most likely a manifestation of the nonuniform spacing of the windings and subsequent nonuniform flow through the matrix. Further testing will be done to resolve this question. We are interested in whether or not the heat and mass transfer coefficients are affected similarly.

Table 6-5. High Rotation Speed Tests

Inlet States							
Test No.	m_{1DA} (kg/s)	t_1 (^oC)	w_1 (g/kg)	m_{2DA} (kg/s)	t_2 (^oC)	w_2 (g/kg)	N (r/h)
HS-1A	0.208	31.0	15.75	0.214	80.0	4.19	135.0
HS-2A	0.209	35.0	15.65	0.213	35.0	4.02	135.0
HS-3A	0.207	31.0	14.17	0.214	80.0	14.00	135.0
HS-1B	0.156	31.0	15.54	0.161	80.0	5.92	135.0
HS-2B	0.158	35.0	15.65	0.161	34.7	5.81	135.0
HS-3B	0.156	31.0	14.00	0.161	80.0	14.02	135.0

Outlet States for Period 1				
Test No.	t_3 (^oC)	w_3 (g/kg)	ε_t	ε_t
HS-1A	68.9	6.99	0.775	0.758
HS-2A	35.9	7.03	--	0.741
HS-3A	68.3	12.78	0.761	--
HS-1B	70.4	7.87	0.804	0.798
HS-2B	36.0	7.75	--	0.803
HS-3B	69.7	13.16	0.790	--

Regenerator Parameters							
Test No.	Heat Transfer			Mass Transfer			Le_o
	C^*	C_r^*	NTU_{to}	C^*	C_r^*	NTU_{wo}	
HS-1A	0.99	5.4	3.55	0.97	2.4	3.40	1.04
HS-2A	--	--	--	0.98	2.4	3.00	1.00
HS-3A	0.97	5.0	3.00	--	--	--	
HS-1B	1.0	7.1	4.14	0.97	3.2	4.07	1.02
HS-2B	--	--	--	0.98	3.2	4.15	0.87
HS-3B	0.97	6.5	3.60	--	--	--	

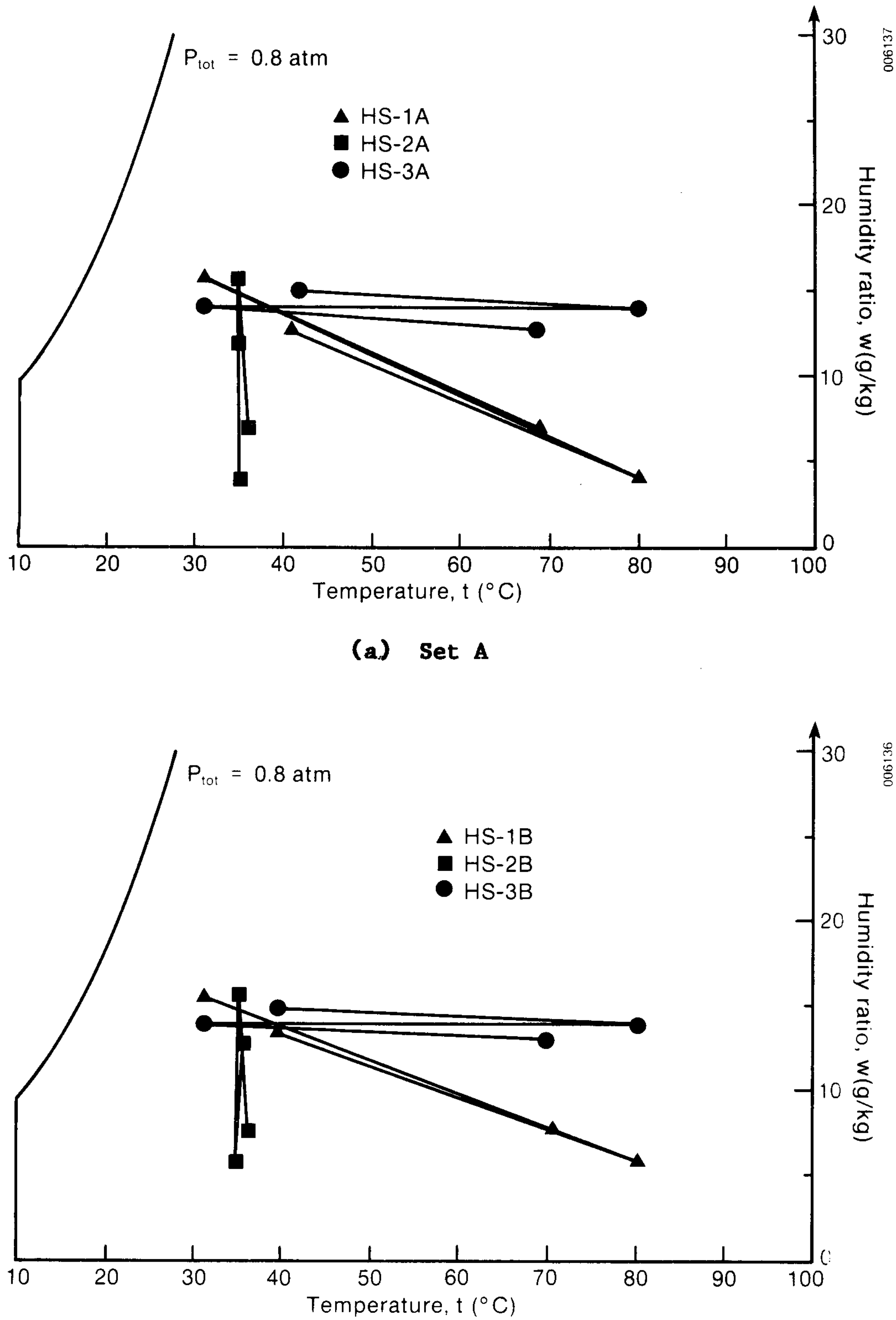

(a) Set A

(b) Set B

Figure 6-9. High Speed Test Results

7.0 CONCLUSIONS

7.1 Facility Status and Preliminary Test Results

SERI's Desiccant Cooling Cyclic Test Facility is assembled and operating. The facility can test bench-scale, rotary solid desiccant dehumidifiers over a wide range of controlled conditions representative of those encountered by solar desiccant cooling systems. We can monitor transient and steady-state operation. The closure of the overall mass and energy balances on the rig are satisfactory for experiments on the first test article; however, improvements will be needed to test higher performance wheels. We can acquire accurate data suitable for model validation.

We can presently control inlet humidity ratios satisfactorily, although the process is somewhat tedious. Velocities at the wheel inlet faces are somewhat nonuniform and highly turbulent. The current dehumidifier appears to provide sufficient pressure drop to even out the flow. However, it may be desirable to redesign the entrance ducting for future tests.

A spirally wound, parallel-passage, rotary dehumidifier using silica gel as the desiccant was constructed and installed in the test loop. Initial tests, single-blow and cyclic, were conducted with satisfactory results. Initial tests indicate that approximately 90% of the silica gel thought to be present is active. The overall Lewis number of the wheel is near unity. However, the nonuniform flow passage spacing seems to be reducing the effective number of transfer units from theory by a factor of 3-4 We will perform further tests to try to understand this.

7.2 Future Work

The test matrix presented in Schultz and Schlepp (1984) will be carried out. This will fully characterize the performance of this first rotary, parallel-passage dehumidifier and allow us to validate the models for this design over a wide range of operating conditions.

Complete validation of the analytical models requires a range of designs to be tested. Based on the results of the first dehumidifier, we will acquire and test other dehumidifier geometries. Several choices are available, including constructing a second parallel-passage dehumidifier with improved passage spacing uniformity (Maclaine-cross 1985). This could be done at SERI or by other commercial manufacturers. A choice will be made as soon as sufficient information is available from the first dehumidifier.

8.0 REFERENCES

Ambrose, C. W., I. L. Maclaine-cross, and E. B. Robson, 1979, The Use of Rotary Regenerative Heat Exchangers for the Conversion of Energy in Buildings, Clayton, Victoria, Australia: Monash University, Dept. of Mech. Engr.

Barlow, R. S., 1982 (Dec.), Analysis of the Adsorption Process and of Desiccant Cooling Systems: A Pseudo-Steady-State Model for Coupled Heat and Mass Transfer, SERI/TR-631-1330, Golden, CO: Solar Energy Research Institute.

Bean, H. S., ed., 1971, Fluid Meters, Their Theory and Application, 6th edition, New York: ASME Research Committee on Fluid Meters.

Booz-Allen and Hamilton, 1981, Evaluation of Residential and Commercial Solar/Gas Heating and Cooling Technologies, GRI-79/0105, Chicago, IL: Gas Research Institute.

Brandemuehl, M. J., 1982, Analysis of Heat and Mass Transfer Regenerators with Time Varying or Spatially Nonuniform Inlet Conditions, Ph.D. thesis, Madison: University of Wisconsin, Dept. of Mech. Engr.

Clark, J. E., 1979, Design and Construction of Thin, Adiabatic Desiccant Beds for Solar Air Conditioning Applications, University of California at Los Angeles.

Cohen, B., A. Levine, and R. Arora, 1983 (Feb.), Field Development of a Desiccant-Based Space-Conditioning System for Supermarket Applications, TE4308-42-83, Chicago, IL: Gas Research Institute.

Howe, R. R., W. A. Beckman, and J. W. Mitchell, 1983 (June), "Commercial Applications for Solar Hybrid Desiccant Systems," Proceedings of the 1983 Annual ASES Meeting, Anaheim, CA: ASES.

Huskey, B., et al., 1982, Advanced Solar/Gas Desiccant Cooling System, GRI 81/10064, Chicago, IL: Gas Research Institute.

Jurinak, J. J., 1982 (Aug.), Open-Cycle Desiccant Cooling: Component Models and System Simulations, Ph.D. thesis, Madison: University of Wisconsin, Solar Energy Laboratory.

Kang, T. S., 1985, "Adiabatic Desiccant Open Cooling Cycles," Master's thesis, Kensington, Australia: University of New South Wales, School of Mech. and Ind. Engr.

Kays, W. M., and A. L. London, 1964, Compact Heat Exchangers, New York: McGraw-Hill.

Kutscher, C. F., and R. S. Barlow, 1982 (Aug.), Dynamic Performance of Packed-Bed Dehumidifiers: Experimental Results from the SERI Desiccant Test Laboratory, SERI/TR-252-1429, Golden, CO: Solar Energy Research Institute.

Maclaine-cross, I. L., 1974, A Theory of Combined Heat and Mass Transfer in Regenerators, Ph.D. thesis, Clayton, Victoria, Australia: Monash University, Dept. of Mech. Engr.

Maclaine-cross, I. L., 1985 (Apr.), Potential Improvements to the SERI Parallel-Passage Dehumidifier Matrix, Internal Branch Report, Thermal Research Branch 252, Golden, CO: Solar Energy Research Institute.

Maclaine-cross, I. L., and P. J. Banks, 1972, "Coupled Heat and Mass Transfer in Regenerators - Prediction Using an Analogy with Heat Transfer," Int'l J. of Heat and Mass Transfer, Vol. 15, pp. 1225-1242.

Macriss, R. A., and T. S. Zawacki, 1982 (Feb.), "High COP Rotating Wheel Solid Desiccant System," Proceedings of the 9th Energy Technology Conference, Washington, DC.

Monier, J. B., W. M. Worek, and Z. Lavan, 1982 (Jan.), Testing of a Cross-Cooled Solar-Powered Desiccant Cooling System, DES-82-1, Chicago, IL: Illinois Institute of Technology.

Penney, T., and I. Maclaine-cross, 1985 (May), Promising Advances in Desiccant Cooling, SERI/TP-252-2683, Golden, CO: Solar Energy Research Institute.

Rousseau, J., 1982 (Nov.), Development of a Solar Desiccant Dehumidifier: Final Summary Report, 82-18944, Torrence, CA: Garrett AiResearch Manufacturing Co.

Schlepp, D., and R. Barlow, 1984 (Sept.), Performance of the SERI Parallel-Passage Dehumidifier, SERI/TR-252-1951, Golden, CO: Solar Energy Research Institute.

Schlepp, D., and K. Schultz, 1984 (Sept.), High Performance Solar Desiccant Cooling Systems: Performance Evaluations and Research Recommendations, SERI/TR-252-2497, Golden, CO: Solar Energy Research Institute.

Schlepp, D., K. Schultz, and F. Zangrando, 1984 (Aug.), Facility Design for Cyclic Testing of Advanced Solid Desiccant Dehumidifiers, SERI/TR-252-2464, Golden, CO: Solar Energy Research Institute.

Scholten, W. B., and J. H. Morehouse, 1983, Active Program Research Requirements: Final Report, McLean, VA: Science Applications, Inc.

Schultz, K., and D. Schlepp, 1984 (Apr.), Experimental Test Plan for Cyclic Testing of Parallel Passage Rotary Desiccant Dehumidifiers, Draft, Golden, CO: Solar Energy Research Institute.

Sharp Co., Product literature, 1982, Nora, Japan.

Strahm, C. S., and S. G. Wilson, 1982a (July), Dehumidifier Seal Development, DET. 21, Highett, Victoria, Australia: CSIRO Division of Energy Technology.

Strahm, C. S., and S. G. Wilson, 1982b (July), Dehumidifier Test Facility Rig Description, Operation, and Maintenance, DET. 22, Highett, Victoria, Australia: CSIRO Division of Energy Technology.

van den Bulck, E., 1983, "Analysis of Solid Desiccant Rotary Dehumidifiers," M.S. thesis, Madison: University of Wisconsin, Dept. of Mech. Engr.

van Leersum, J., et al., forthcoming, "Comparison of the Results from Experiments on a Rotary Particulate

Bed Dehumidifier with Those from a Numerical Model," submitted to ASME J. of Solar Energy Engr.

van Leersum, J. G., and D. J. Close, 1982 (June), Experimental Verification of Open Cycle Cooling System Component Models, Draft, Madison: University of Wisconsin.

Venhuizen, D., 1984 (Oct.), "Solar King's Cooling Gambit," Solar Age, Vol. 9, No. 10, p. 25-27.

Wurm, J., et al., 1979 (Nov.), Solar-MEC Development Program: Semiannual Progress Report, COO-4495-23, Chicago, IL: Institute of Gas Technology.

SELECTED DISTRIBUTION LIST

William M. Anderson
Anderson Consulting
7605 E. Windlawn Way
Parker, CO 80134

Carl Bergt
Trane Systems Engineering Co.
6200 Troup Highway
Tyler, TX 75711

Kennard L. Bowlen
Cargocaire Engineering Corp.
79 Monroe St.
Amesbury, MA 01913

Glen Chinery
Tennessee Valley Authority
217 Power Board Bldg
Chattanooga, TN 37401

James Coellner, Director R&E
American Solar King Corp.
700 Loop 340 South
Waco, TX 76710

Barry Cohen
Thermal Products Division
ThermoElectron Corporation
45 First Avenue
Waltham, MA 02154

Kirk Collier, Ph.D.
Everscope, Inc.
4886 W. Port au Prince
Glendale, AZ 85306

Keith Davidson
Gas Research Institute
8600 West Bryn Mawr Avenue
Chicago, IL 60631

Robert Dikkers
National Bureau of Standards
Technology B-148
Washington, DC 20585

Michael Epstein
Fauske & Associates, Inc.
162070 West 83rd Street
Burr Ridge, IL 60521

Phillip Fairey
Florida Solar Energy Center
300 State Road, 401
Cape Canaveral, FL 32920

A. Hunter Fanney, Ph.D.
Bldg. 226, Room B310
National Bureau of Standards
Washington, DC 20234

Stephen D. Fitch
Bry-Air
P. O. Box 795
Sunbury, OH 43074

Anthony Fraioli, Ph.D.
Argonne National Laboratory
9700 South Cass Avenue
Argonne, IL 60439

Paul Gandhidasan, Ph.D.
Dept. Mechanical Engineering
Texas A&M University
College Station, TX 77843

John Goldsmith
U.S. Department of Energy
Route CE-311, Room 5H065
1000 Independence Ave., S.W.
Washington, DC 20585

William C. Griffiths
Midland Ross Corporation
P. O. Box 791
New Brunswick, NJ 08903

R. Harkins
ASES
2030 17th St.
Boulder, CO 80302

Richard B. Hayter, Ph.D.
Engineering Extension
Ward Hall, Kansas State University
Manhattan, KS 66506

Anthony Hines, Ph.D.
College of Engineering
Oklahoma State University
Stillwater, OK 74078

Ralph Johnson
NAHB Research Foundation, Inc.
3720 T St., N.W.
Washington, DC 20007

Robert Jones
Los Alamos National Lab
P.O. Box 1663
Mail Stop H577
Los Alamos, NM 87545

K. LaPorta
SEIA
1156 15th St., N.W., Suite 520
Washington, DC 20005

Zalman Lavan, Ph.D.
Illinois Institute of Technology
Department of Mechanical Engineering
Illinois Institute of Technology
Center
Chicago, IL 60616

Robert LeChevalier
U.S. Department of Energy
San Francisco Operations Office
1333 Broadway
Oakland, CA 94612

George O. G. Löf, Ph.D.
Colorado State University
Solar Energy Applications Lab
Fort Collins, CO 80523

Ian Maclaine-cross, Ph.D.
University of New South Wales
School of Mechanical and Industrial
Engineering
P.O. Box 1
Kensington, NSW 2033 Australia

John Mitchell, Ph.D.
University of Wisconsin-Madison
Engineering Research Building
1500 Johnson Drive
Madison, WI 53706

Jeff Morehouse
Department of Mechanical Engineering
University of South Carolina
Columbia, SC 29208

Frederick Morse, Ph.D.
U.S. Department of Energy
Route CE-31, Room 5H-095
1000 Independence Ave., S.W.
Washington, DC 20585

Stanley A. Mumma
104 Engineering "A" Building
University Park, PA 16802

Yves O. Parent
Industrial Chemicals Research
Davison Chemical Division
W. R. Grace & Co.
Washington Research Center
7379 Route 32
Columbia, MD 21044

David Pellish
U.S. Department of Energy
Forrestal Building, Room 5H-041
1000 Independence Ave., S.W.
Washington, DC 20585

D. M. Ruthven, Ph.D.
University of New Brunswick
P. O. Box 4400
Fredericton, New Brunswick
Canada E58 5A3

William Seaton
ASHRAE
1791 Tullie Circle, N.E.
Atlanta, GA 30329

M. Wahlig, Ph.D.
Lawrence Berkeley Laboratories
University of California
1 Cyclotron
Berkeley, CA 94720

Alex Willman
ACEC Resource and Management
Foundation
1015 15th Street, N.W.
Washington, DC 20005

Byard Wood, Ph.D.
Dept. of Mechanical & Aerospace Eng.
Arizona State University
Tempe, AZ 85287

Document Control Page	1. SERI Report No. SERI/TR-252-2718	2. NTIS Accession No.	3. Recipient's Accession No.

4. Title and Subtitle
SERI Desiccant Cooling Test Facility: Status Report
Preliminary Data on the Performance of a Rotary Parallel-Passage Silica-Gel Dehumidifier

5. Publication Date
April 1986

6.

7. Author(s)
Kenneth J. Schultz

8. Performing Organization Rept. No.

9. Performing Organization Name and Address
Solar Energy Research Institute
1617 Cole Boulevard
Golden, Colorado 80401

10. Project/Task/Work Unit No.
3023.210

11. Contract (C) or Grant (G) No.
(C)
(G)

12. Sponsoring Organization Name and Address

13. Type of Report & Period Covered
Technical Report

14.

15. Supplementary Notes

16. Abstract (Limit: 200 words)

This report describes the SERI Desiccant Cooling Test Facility. The facility can test bench-scale rotary dehumidifiers over a wide range of controlled conditions. We constructed and installed in the test loop a prototype parallel-passage rotary dehumidifer that has spirally wound polyester tape coated with silica gel. The initial tests gave satisfactory results indicating that approximately 90% of the silica gel was active and the overall Lewis number of the wheel was near unity. The facility has several minor difficulties including an inability to control humidity satisfactorily and nonuniform and highly turbulent inlet velocities. To completely validate the facility requires a range of dehumidifier designs. Several choices are available including constructing a second parallel-passage dehumidifier with the passage spacing more uniform.

17. Document Analysis

a. Descriptors Cooling ; Dehumidifiers ; Desiccants ; Test Facilities ; Testing

b. Identifiers/Open-Ended Terms

c. UC Categories
59a

18. Availability Statement
National Technical Information Service
U.S. Department of Commerce
5285 Port Royal Road
Springfield, Virginia 22161

19. No. of Pages
58

20. Price
A04

Form No. 0069 (3-25-82)